ELSEVIER

Journal of Nuclear Materials 241–243 (1997) 1–26

journal of nuclear materials

Section 1. Invited Papers

Plasma–wall interactions in ITER

R. Parker [a,*], G. Janeschitz [a], H.D. Pacher [b], D. Post [a], S. Chiocchio [a], G. Federici [a], P. Ladd [a], ITER Joint Central Team [a], Home Teams [b]

[a] *ITER Joint Central Team, Garching Joint Work Site, Boltzmannstraße 2, 85748 Garching, Germany*
[b] *ITER EU Home Team, Boltzmannstraße 2, 85748 Garching, Germany*

Abstract

This paper reviews the status of the design of the divertor and first-wall/shield, the main in-vessel components for ITER. Under nominal ignited conditions, 300 MW of alpha power will be produced and must be removed from the divertor and first-wall. Additional power from auxiliary sources up to the level of 100 MW must also be removed in the case of driven burns. In the ignited case, about 100 MW will be radiated to the first wall as bremsstrahlung. Allowing the remaining power to be conducted to the divertor target plates would result in excessive heat fluxes. The power handling strategy is to radiate an additional 100–150 MW in the SOL and the divertor channel via a combination of radiation from hydrogen, and intrinsic and seeded impurities. Vertical targets have been adopted for the baseline divertor configuration. This geometry promotes partial detachment, as found in present experiments and in the results of modelling runs for ITER conditions, and power densities on the target plates can be ≤ 5 MW/m^2. Such regimes promote relatively high pressure (> 1 Pa) in the divertor and even with a low helium enrichment factor of 0.2, the required pumping speed to pump helium is ≤ 50 m^3/s. An important physics question is the quality of core confinement in these attractive divertor regimes. In addition to power and particle handling issues, the effects of disruptions play a major role in the design and performance of in-vessel components. Both centered disruptions and VDE's produce stresses in the first-wall/shield modules, backplate and the divertor wings and cassettes that are near or even somewhat in excess of allowables for normal operation. Also plasma–wall contact from disruptions, including at the divertor target, together with material properties are major factors determining component lifetime. Considering the potential for impurity contamination and minimizing tritium inventory as well as thermomechanical performance, the present material selection calls for carbon divertor targets near the strike point, tungsten on the rest of the target and on the baffle where the charge-exchange flux could be high, and beryllium elsewhere. All three materials and relevant joining techniques are being developed in the R&D program and the final selection for the first assembly will be made at the end of the EDA.

Keywords: ITER; Divertor modelling; Pumping and fuelling; Wall erosion; Wall particle retention

1. Introduction

Since the early phase of the of the ITER conceptual design activities, the design of in-vessel components for ITER, in particular the divertor and first wall, has been recognized as among the most challenging problems confronting the ITER design. Not only must the invessel components be capable of exhausting heat and particle fluxes at levels near the limit of what is technologically feasible, they must do so in an environment subject to frequent plasma disruptions which, through the resulting electromagnetic forces, produce huge mechanical loads that must be safely reacted by the supporting structure. Such disruptions also deposit large energy fluxes on the plasma facing components (PFC's), which can lead to melting or sublimation of the surface, and possibly damage to the cooling system, thereby limiting lifetime of the PFC's and/or requiring intervention for repair. Nevertheless, partially as a result of progress made in an intensive physics R&D effort launched near the beginning of the

* Corresponding author. Tel.: +49-89 3299 4134; fax: +49-89 3299 4444.

PII S0022-3115(96)00491-6

EDA, as well as further advances in materials and high-heat-flux technology R&D, potentially robust solutions for the divertor and first wall design for ITER have emerged and their description and performance is the main subject of this paper.

A cross-sectional view of ITER is shown in Fig. 1 and the parameters of a representative operating point are given in Table 1 [1]. From the table it can be seen that the average neutron wall loading is 1 MW/m^2, the recommended value for testing of DEMO-relevant blanket modules. For the ignited plasma whose parameters are given in the table, this implies an average thermal load of 0.25 MW/m^2. The design also has the capability for a driven burn using an auxiliary heating capability of up to 100 MW, in which case the average thermal wall loading would increase to 0.33 MW/m^2. While such values are not difficult to accommodate by the first wall, the exhaust power is largely transported to the divertor, where in the normal high-recycling regime it is deposited in a relatively small area on the divertor target plates. Power densities there could then approach or even exceed 30 MW/m^2, an unacceptably high value.

The basic strategy for coping with the power exhaust problem is illustrated in Fig. 2 which shows a large fraction of the power being radiated before it is transported to the divertor. In typical discharge conditions, 100 MW or about 1/3 of the α power is unavoidably radiated directly to the first wall by bremsstrahlung. Of the remaining 200 MW, 100–150 MW is to be removed by radiation from impurities, both intrinsic (He, Be, C) and seeded (Ne, Ar, ...), and also hydrogen, in the edge mantle, i.e., the region just inside the separatrix, in the SOL, and by charge-exchange with neutrals, which occurs mainly near the divertor plates. In this way the power flux to the target can be reduced to the range 5–10 MW/m^2 which is a reasonable nominal value for the target design. Furthermore, based on modelling results for these conditions (Section 2.1), the divertor channel is expected to partially detach, and the peak power density would then fall below the 5–10 MW/m^2 level. In order to promote detachment, and also to encourage the possibility of substantial power loss from the divertor at moderately low power density, a relatively large fraction of the in-vessel space is devoted to the divertor structure (Section 2.2).

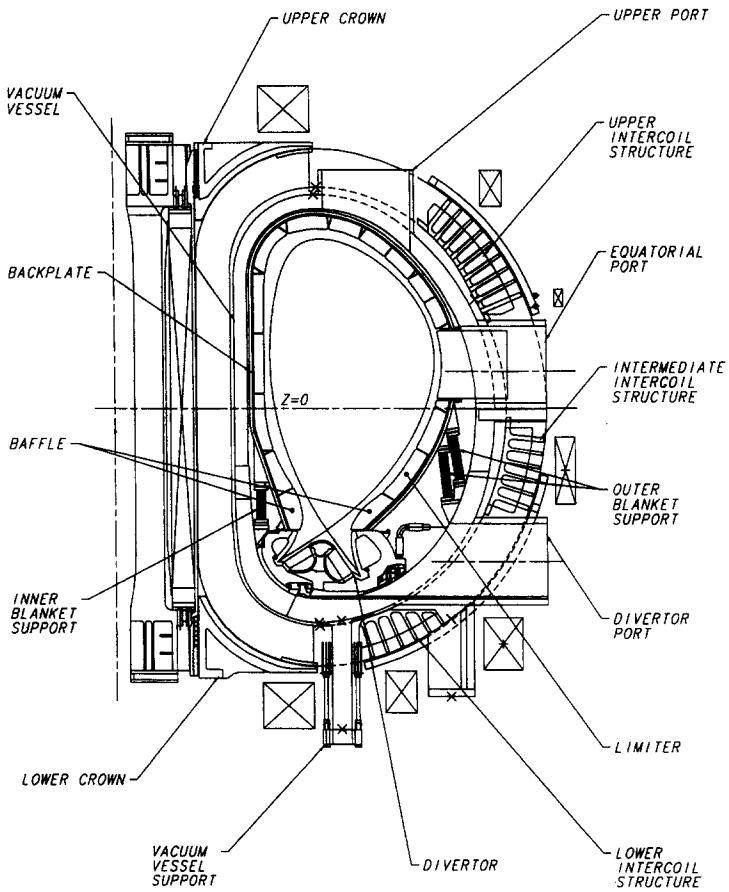

Fig. 1. Cross-section of the ITER tokamak design showing the divertor and first-wall/shield layout.

Table 1
Parameters and a representative operating point for the ITER design as described in the interim design report. The confinement time used in obtaining the operating point is that derived for ELMy H-Mode by the ITER confinement database and expert group [2]

Parameter	Symbol	Value
Major, minor radius	R, a	8.14, 2.8 m
Plasma elongation	κ_{95}, κ_x	~ 1.6, ~ 1.75
Plasma triangularity	δ_{95}	~ 0.24
Nominal plasma current	I	21 MA
Toroidal field	B	5.68 T (at $R = 8.14$m)
MHD safety factor	q_{95}	3.05
Volume-averaged temperature	T	10.5 keV
Volume-averaged density	n	1.3×10^{20} m^{-3}
Impurity fractions	f_{Be}, f_{He}	0.02, 0.14
Effective charge	Z_{eff}	1.5
Normalized beta	β_n	2.4
Fusion power (nominal)	P_{fus}	1.5 GW
Average neutron wall loading	Γ_n	~ 1 MW/m^2
Burn duration	t_{burn}	1160 s
Plasma magnetic, thermal energy	W_{mag}, W_{th}	1.1, 1.2 GJ

Disruptions pose a major problem for the design of all in-vessel components. Despite rapid progress during the last 20 years of tokamak development, disruptions still occur frequently in all operating tokamaks and it must be assumed that this will be the case for ITER. Consistent with present experience, it is expected that ITER will have a relatively high disruption frequency (~ 30%) in the first few years of operation, but that the frequency should decline to perhaps < 10% as the operation becomes less exploratory toward the end of the Basic Performance Phase. Three basic types of disruptions are foreseen: one in which the plasma first undergoes a partial or full thermal quench followed by a rapid current quench with small vertical displacement (type 1); a second which is similar to type 1 except that there is a period of substantial vertical movement before or during the current quench (type 2); and a third in which there is first a loss of vertical control followed by a large vertical displacement of the plasma which still contains most of its thermal energy (type 3). As a result of disruptions, substantial currents will be induced in the first-wall and shielding-blanket structure, as well as in the divertor, and these currents produce forces which must be carefully taken into account in the design.

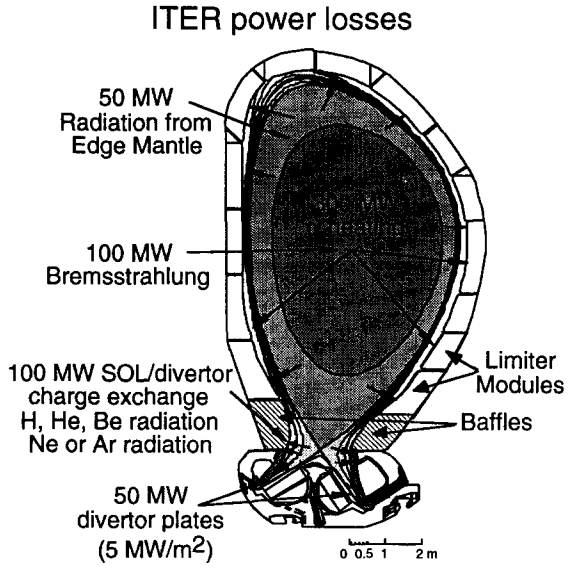

Fig. 2. Schematic division of power flowing to the first wall and divertor.

The first wall is integrated into shielding-blanket modules which are in turn connected to a 100 mm thick toroidal shell or 'backplate' (see Fig. 1). The electromagnetic pressure resulting from each of the three types of disruptions is transmitted from the wall through the module to the backplate, where it is at least partially reacted as hoop stress. However, in the case of type 2 and 3 disruption, net vertical and horizontal forces (~ 150 MN and ~ 50 MN) arise which will be transmitted to the vacuum vessel through the blanket support legs. A particularly difficult design issue is the attachment of the blanket modules to the backplate; on one hand, the modules must be removable for repair (and also for conversion to the breeding blanket required for the extended performance phase) by reasonably straightforward remote handling operations, and on the other hand, the attachment must be extremely robust in order to cope with the enormous disruption forces. The modular design developed in the last two years of the EDA appears optimum in meeting the stringent design requirements. More details regarding the design and an analysis of its ability to safely react the limiting disruption mechanical loads are presented in Section 3.

An additional effect of disruptions is the energy released to the plasma facing components and its effect on both structural integrity and lifetime. In the case of a thermal quench which is expected to occur when the plasma is diverted (type 1), most of the plasma thermal energy is expected to be dumped onto the divertor plates and significant material can be lost by melting or sublimation. The frequency and intensity of such events, as well as the material, are a determining factor in the expected lifetime of the divertor target (Section 4). However, since the divertor target thermo-hydraulic system is designed for very high heat fluxes, it is expected that no structural damage should occur. For type 2 and 3 disruptions, in which substantial vertical motion occurs, plasma–wall contact will occur and an energy flux to the wall of 20–60 MJ/m^2 is anticipated. The heat removal system for the first-wall necessarily has far lower capacity than that for the divertor, and the possibility for burnout exists. A critical parameter is the duration over which the energy is

released, the most dangerous time being about one second, near the thermal equilibration time of the wall. For shorter times, steady-state conditions are not reached and the hydraulic system is protected by the walls thermal inertia. For somewhat longer times, the maximum heat flow to the coolant is limited by the heat flux that can be supported by the maximum thermal gradient in the wall. Since both the mechanical and thermal effects of type 2 and 3 disruptions are critical to the design, mitigation measures against these disruptions are being vigorously pursued in the physics R&D program.

2. Divertor design and performance

The ITER divertor is required to exhaust the major part of the alpha particle power, exhaust the He ash rapidly enough to keep the He concentration in the main plasma below 10%, keep the neutral (DT, He,...) leakage from the divertor to the main chamber below ~ 30 Pa m^3/s, achieve acceptable component lifetimes with a goal of greater than 3000 full power discharges which include up to 1000 high power transients, withstand the thermal- and electromagnetic loads during disruptions (goal 1000 disruptions at full power) and be designed to be exchangeable by remote handling within 6 months. The high power transients are events anticipated to be caused by power excursions or other changes in plasma conditions, which temporarily 'burn through' the normally detached or partially detached plasma conditions at the divertor plates. They will result in transient heat loads of ~ 20 MW/m^2 lasting up to 10 s while the thermal flux expected for normal plasma conditions is 5 MW/m^2.

2.1. Physics concept and modelling results

To meet these goals, it is necessary to have both a robust engineering design and to achieve plasma operational regimes which (1) reduce the heat loads on the plasma facing components to acceptable levels $Q_{\text{Target}} \sim 5$ MW/m^2 without unduly increasing the particle flux and (2) provide adequate helium partial pressures (> 0.01 Pa) in the divertor for He exhaust. Therefore the divertor plasma has to be operated so that (1) most of the power crossing the separatrix is spread out over the walls of the main chamber and divertor chamber by radiation and charge exchange before the plasma reaches the target plates and (2) most of the recycling neutral gas is confined in the divertor chamber, producing high neutral pressures there of 0.3 to 10 Pa. The basic physics picture of how detached or semi-detached regimes apply to ITER is described in [3]. The important atomic processes important for accessing these regimes have been identified and described in [4].

During the last few years regimes of this type have been achieved on many divertor tokamaks [5–9] and have been reported and discussed in the ITER divertor expert group meetings. A basic physics picture for these regimes and how they apply to ITER has emerged. Detachment is achieved by either strong gas puffing or by a combination of impurity seeding (N, Ne, Ar) and gas puffing. Strong gas puffing enhances the radiation of intrinsic impurities as well as the plasma–neutral interaction in the divertor and impurity seeding adds additional radiating impurities. For all of the major divertor experiments, a reduction of the peak heat flux on the divertor plates by a factor of up to five or more (Figs. 3 and 4) [9–13] could be attained even for the maximum available heating power. In general, as the gas puffing rate was increased, the ionization front (5 eV boundary) moved from the target to near the X-point where all the radiation was concentrated. However, recent experiments indicate that the location of the ionization front as well as the radiation loss region can be controlled by feedback on the gas and impurity fuelling [11,14]. Discharges where the radiating area is distributed along the separatrix between the target plate and the X-point are detached only near the separatrix, remaining attached in the outer region of the SOL. The existence of this 'semi-detached' regime does not appear to depend on the divertor geometry. It has been observed in vertical target as well as flat plate divertors [15,16]. However, the threshold density and impurity concentration for detachment depends on the power flux into the divertor and on the divertor geometry (including the amount of baffling) [15].

Gas puffing (which increases the radiation of the mostly low-Z intrinsic impurities) appears to produce detachment at slightly higher densities than with medium-Z impurity injection (e.g., Ne). However, with gas puffing and intrinsic impurities, the radiation is concentrated at the X-point and below. With medium-Z impurity fuelling, a substantial fraction of the power is radiated in the mantle of the core plasma which reduces the power flux into the divertor. Once the temperature at the divertor plates is low enough for a significant fraction of neutrals to be able to escape the plasma fan, the neutral pressure in the divertor area starts to rise promoting radiation and momentum losses. The consequent detachment usually starts at the inner divertor channel due to the well known target power asymmetry [12,14]. However, when the outer divertor starts to detach, the target power asymmetry disappears.

All experiments find that completely detached plasmas (with the ionization front at the X-point) have confinement that is close to L-mode. With detached plasmas, the recycling neutrals are not as well confined near the divertor as with attached plasmas. The neutral pressure around the main plasma is therefore higher and the confinement degrades [17]. The confinement is better with the injection of medium-Z impurities such as Ne than with gas puffing alone (e.g., the CDH-mode [7,11]). The neutral pressure is lower since less gas puffing is necessary to achieve detachment but the observed impurity levels are too high (Z_{eff} values > 2.5) for ITER. At this time, a detached discharge

that simultaneously has good confinement and a low Z_{eff} has not yet been observed experimentally. However, in contrast to ITER most of the present divertor configurations have either no baffle at all or have rather large bypass leaks which allow neutrals to escape to the main chamber to the divertor. This leakage also limits the neutral pressure in the divertor and thus delays the onset of detachment. Most of the major divertor experiments will modify their divertors to enhance the retention of neutrals in the divertor chamber (becoming more like the highly baffled ITER design).

While detached operation would have the lowest heat and particle loads, operation with partially detached plasmas in ITER would result in higher temperatures and therefore ionization rates in the outer region of the SOL and thus help to provide a plasma 'seal' and thus reduce the flux of neutrals away from the divertor plate toward the main plasma. This regime might therefore have better confinement performance since it is known that high neutral pressure in the main chamber can lead to confinement degradation. It would result in slightly higher power fluxes on the ITER divertor targets (up to 10 MW/m^2) and shorter component lifetimes than a fully detached regime (Section 4.1) but is a feasible regime for ITER.

These experimental observations together with a variety of models (analytic and one and two dimensional codes) and an edge data base are being used to assess the performance of the ITER divertor. The goal for ITER divertor operation is that energy losses from the main plasma and divertor must be high enough so that the peak heat flux on the divertor plates is in the order of 5 MW/m^2 or about 50 MW in total. The total heating power in ITER consists of 300 MW of alpha particle heating and up to 100 MW of auxiliary heating. Energy losses due to bremsstrahlung from the plasma center, impurity line radiation from the 'mantle' at the plasma edge inside the separatrix, radiation from the scrape-off layer and divertor plasma due to H, He, Be and/or C, and Ne, Ar, or Kr and charge exchange

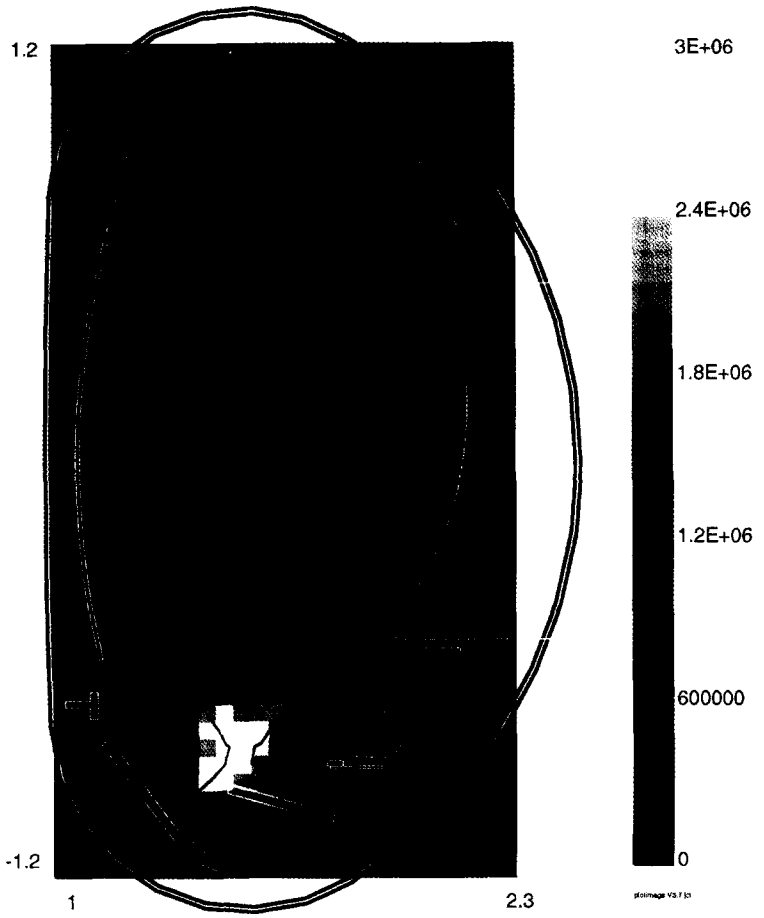

Fig. 3. Contours of the radiation losses (W/m^3) in ASDEX Upgrade measured by tomographic analysis of bolometer data for a CDH regime plasma produced with strong neon and deuterium fuelling [11].

losses are all potential processes which can reduce the power on the divertor plates. The power balance foreseen for ITER is summarized in Table 2.

For a Z_{eff} of about 1.6 with $n_{He}/n_e \sim 10\%$, $n_{Be}/n_e \sim 1\%$ and 0.3% Ne, the bremsstrahlung radiation from the plasma core will be about 100 MW [18]. Bremsstrahlung losses play a much larger role in ITER than in present experiments because the ITER alpha particle heating density of 0.13 MW/m^3 is much lower than the auxiliary heating power density of ~ 1 MW/m^3 in present experiments, while the high density and temperatures in ITER increase the bremsstrahlung emission.

The remaining 200 to 300 MW of power must be reduced to ~ 50 MW by impurity radiation and other atomic processes. The plasma electron temperature in the main plasma ranges from 200–500 eV at the separatrix to 15–20 keV at the plasma center. The electron temperature in the SOL and divertor plasma ranges from 1–20 eV near

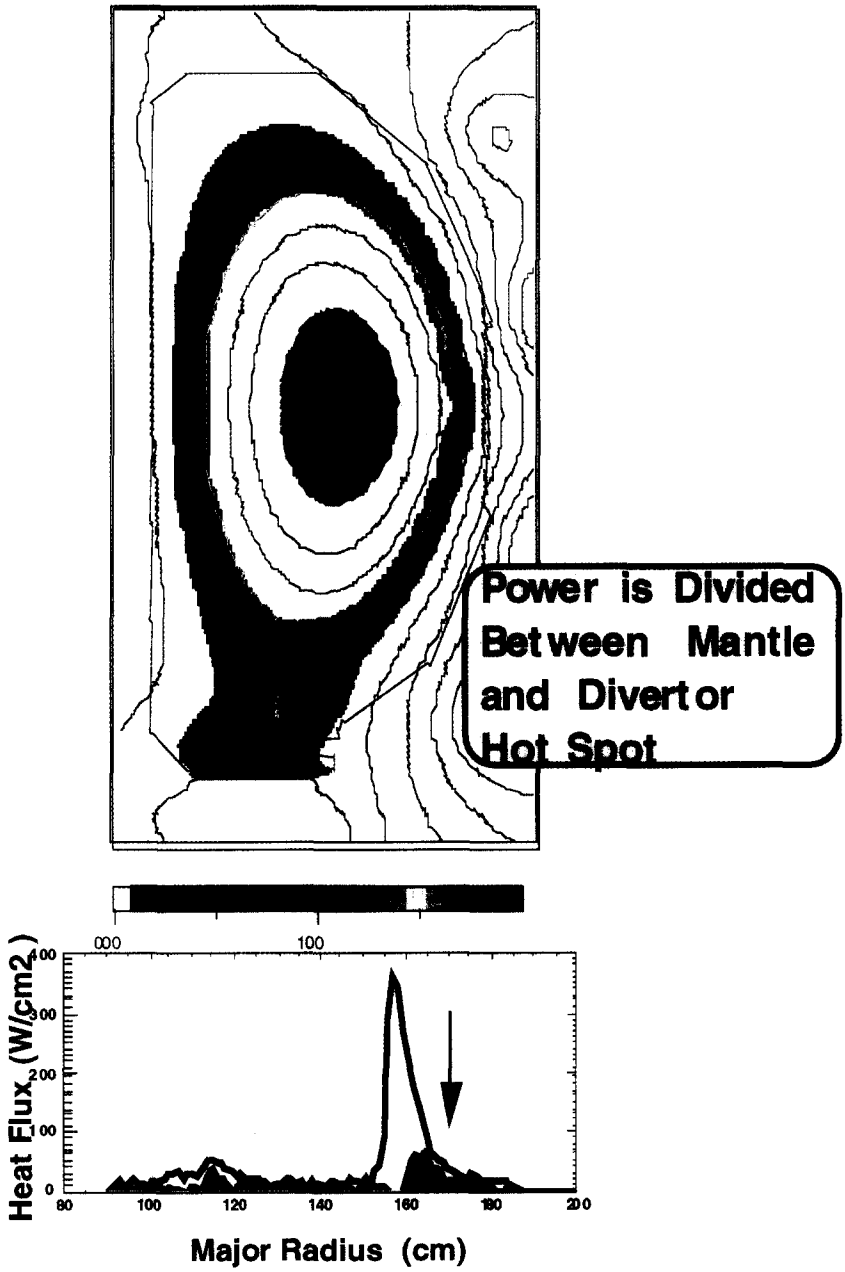

Fig. 4. Radiation loss rates (MW/m^3) in DIII-D produced with strong D_2 and neon fuelling and the heat loads on the divertor plates before (upper curve) and after (shaded) neon fuelling [6].

Table 2
ITER power balance sum

Process	Power (MW)	(Range)
Alpha heating (plus auxiliary heating)	300	(300–400)
Bremsstrahlung from plasma core	100	(60–120)
Mantle (Ne, Ar or Kr)	50	(50–150)
Divertor/SOL losses (CX, H, He, Be/C, Ne/Ar/Kr)	100	(50–200)
Divertor plate	50	(50–100)

the divertor plate to 20–500 eV near the separatrix at the midplane. Higher-Z impurities such as Ar and Kr are therefore optimal for radiation in the plasma mantle (Fig. 5), whereas a somewhat broader selection of impurities are appropriate for the SOL and divertor.

Calculations using a simple analytic model indicate that the radiation in the plasma mantle will be in the 40 to 100 MW range for neon and argon, depending on the plasma transport and the edge density, for a ΔZ_{eff} of ~ 0.3 due to these impurities [18]. More detailed calculations using the GTWHIST $1\frac{1}{2}$ dimensional tokamak transport code with multi-species impurity transport indicates that the radiation from the plasma edge 'mantle' inside the separatrix can be between 50 and 150 MW with acceptable plasma performance [18,19]. For example, the mantle radiation is about 100 MW with 0.1% of Argon (Fig. 6) whereas 0.01% Kr produces roughly equivalent results. For the highest levels of radiation from the mantle and central plasma, 20 to 30 MW of auxiliary heating is required to compensate for the increased core radiation. Not all of the power can be radiated from the mantle because some power is needed to exceed the H-mode threshold and avoid the H → L transition. Depending on the scaling, the H-mode threshold power for ITER varies from 40 to 150 MW. For the highest H-mode threshold scalings, the mantle radiation should not exceed ~ 50 MW and the divertor and SOL would have to handle 150 MW.

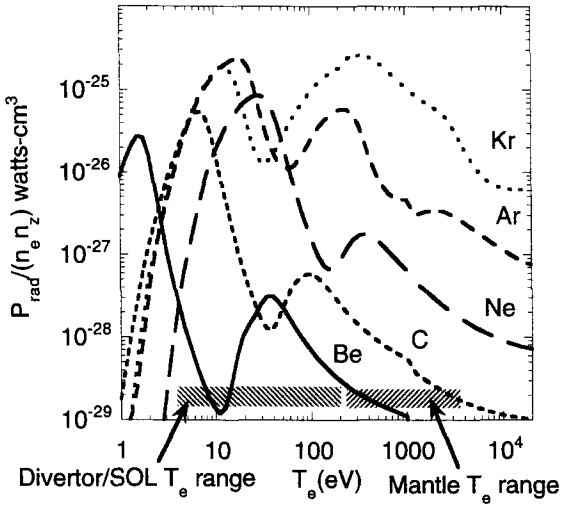

Fig. 5. Radiation loss coefficients for representative elements in ITER.

The power to the divertor will therefore be between 50 and 250 MW with a nominal value of 150 MW, which needs to be reduced by radiation and charge exchange to 50 MW on the divertor plate. Analytic models similar to the ones used for the mantle indicate that for a mid-plane density of 5×10^{19} m^{-3}, the impurity radiation levels with about 0.33% Ne or 0.1% Ar ($\Delta Z_{\text{eff}} \approx 0.3$) will be 25 to 35 MW [18]. These estimates do not include effects that would increase the radiation losses such as two dimensional heat conduction, charge exchange recombination and impurity recycling. Sufficiently rapid impurity recy-

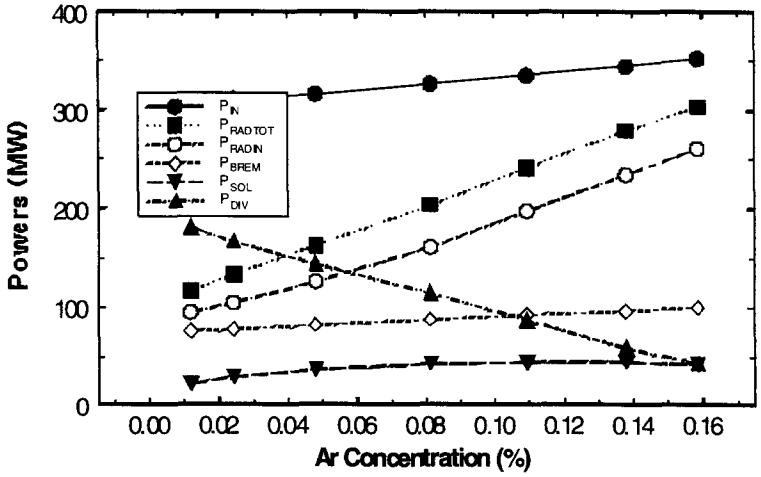

Fig. 6. Power balance calculated using the GTWHIST code. P_{INPUT} is the total input power, P_{RADTOT} is the total radiated power, P_{RADIN} is the radiated power from inside the separatrix, P_{BREM} is the bremsstrahlung loss from the plasma center, P_{SOL} is the power radiated from the SOL and divertor plasma (outside the separatrix), and P_{DIV}-plate is the power on the divertor plates [19].

cling [4] or a neutral fraction of 3×10^{-4} would increase the neon radiation levels to 70 MW. The contribution of many of these effects has been evaluated with 2D divertor models (B2 and UEDGE) with simplified impurity transport algorithms. A UEDGE [20] calculation with a uniform neon fraction of 0.33% indicates that the neon radiation is about 100 MW with another 20 MW of radiation due to hydrogen [18]. Calculations with the B2 code [21] using a multi-species transport model for neon without the ion temperature thermal force indicate that the Ne radiation level will be about 70 MW for similar conditions and 0.1% Argon produces equivalent results. Adding the line radiation from 'intrinsic' impurities such as He, Be and C and from hydrogen, and charge exchange losses, these estimates indicate that 100 to 150 MW can be radiated from the divertor with Ne or Ar with ($\Delta Z_{\text{eff}} \approx 0.3$) if the impurity distribution is fairly uniform [18].

These calculations do not include the effect of the ion thermal force, which tends to lower the impurity density where most of the power is flowing by pushing the impurities up the ion temperature gradient toward the mid-plane. This happens in particular near the separatrix where the temperature gradient is strongest. They then diffuse further out into the SOL where they flow back toward the divertor plate. This can significantly reduce the impurity radiation. This effect is especially strong when flow reversal occurs near the separatrix and the plasma flows back toward the main plasma from the divertor so that the friction force also depletes the impurities near the separatrix [22]. The B2/EIRENE [23] and UEDGE [20] codes have been used to study the impact of these effects. Both of these codes are being extensively validated by their use in analyzing divertor data [10,24,25]. The status of the validation of divertor models is reviewed in a paper by Loarte [25] given at this meeting. The B2/EIRENE code has been used to analyze the experimental data from detached ASDEX Upgrade [24,26] and the UEDGE code has been used to analyze data from DIII-D [27]. The UEDGE calculations indicate for ITER that the neon radiation will be 20 to 40 MW for an upstream Ne concentration of 0.4–0.6% depending on the cross field transport [18]. The hydrogen radiation losses are about 15 MW and are relatively independent of the neon level. A MARFE forms for neon concentrations above 0.8% and the calculation cannot be carried further.

Calculations with the B2/EIRENE code for ITER [23] indicate that with a power across the separatrix of 200 MW, a separatrix density of 4.4×10^{19} m^{-3} and a helium concentration of 10%, total radiation levels of up to 160 MW can be obtained for neon concentrations in the plasma core between 0.5 and 1% (Fig. 7) and the power to each divertor target is reduced to about 20 MW [23]. The peak power on the divertor plates drops from 10 MW/m^2 with 0.5% neon to about 1.4 MW/m^2 with 1% neon (Fig. 8). The neon radiation losses are 40 to 50 MW, roughly consistent with the UEDGE results (Fig. 9). The thermal force and flow reversal reduce the neon radiation below that calculated for a uniform neon concentration. However, the radiation losses are very high because the hydrogen radiation is more than 100 MW (Fig. 9). A region of cold, dense plasma forms along the separatrix and near the X-point. Volume recombination is very strong in this region and the neutral and ion densities there are both 10^{20}–10^{21} m^{-3}. The regions where ionization and recombination occur are adjacent forming a 'virtual target' and the recycling takes place locally within the plasma. Each

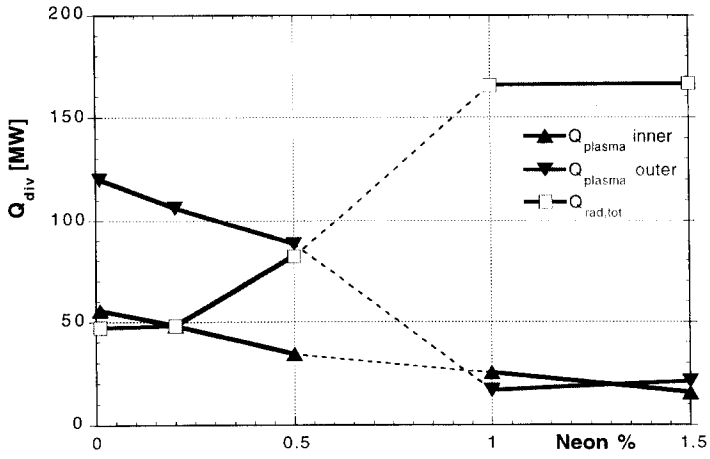

Fig. 7. Calculated B2/EIRENE total radiation losses (neutral, ion, bremsstrahlung) and total power to the inner and outer divertor plates (both plasm and neutrals: conduction, ion convection, surface recombination, neutral convection, molecular dissociation) as a function of the neon concentration at the core-edge interface for ITER [23].

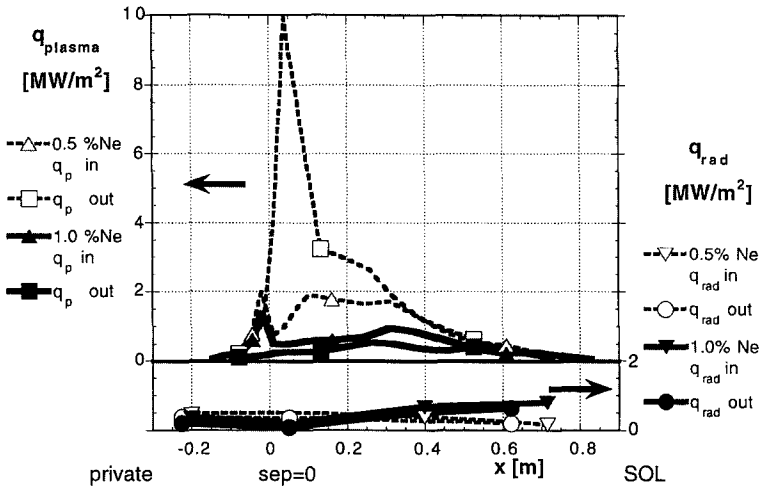

Fig. 8. Profile of the power per unit area due to particles and to radiation on the inner and outer divertor plates for a neon concentration at the core-edge interface of 0.5% and of 1% [23].

ionization and each recombination event radiates about 10 eV. The radiation emissivity in this region is in the 3 to 10 MW/m^3 range. This type of recycling is fundamentally different from recycling off a solid surface where the ionization energy is deposited on the plate for each recombination.

This type of divertor plasma behavior is similar to the results of recent experiments with detached plasmas in Alcator C-Mod in which the total energy losses as measured by bolometers rise strongly during detachment, but the impurity radiation is reported to remain relatively constant [13]. Volume recombination has been reported in many experiments (e.g., Alcator C-Mod [13]) This regime is very promising for ITER operation, but needs further modelling studies and experimental validation. A 1% neon concentration in the core, together with the helium and intrinsic impurities, will likely produce unacceptable penalties in plasma performance but concentrations of 0.5% are probably acceptable.

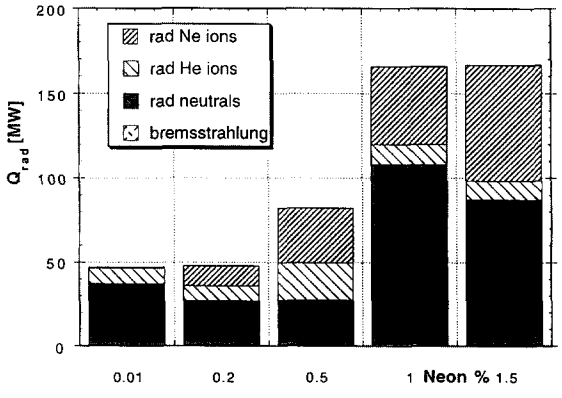

Fig. 9. Calculated B2/EIRENE radiation loss contributions from different sources (neutrals, Ne ions, He ions) as a function of the neon concentration at the core-edge interface for ITER [23] (Bremsstrahlung in SOL negligible).

Calculations with the EDGE2D/NIMBUS code indicate that with light seeding with nitrogen, due to the strong cross field transport which is assumed, based on JET data, modest radiation losses are sufficient to reduce the peak heat loads on the divertor plates to acceptable levels [28].

The effects of flow reversal and the ion thermal force can be overcome if the plasma flow toward the divertor plate and the associated friction force on the impurities are sufficiently strong. A sufficiently strong flow could potentially result in higher impurity concentrations in the divertor than in the main plasma and significantly enhanced radiation levels in the divertor. The plasma flow toward the divertor can be increased by intense gas puffing in the main chamber and pumping in the divertor. Preliminary estimates of the flow rates needed range from 200 to 500 Pa m^3 s^{-1} for ITER. The present capability of the gas fuelling system is 200 Pa m^3 s^{-1} (Section 2.5) but it can be extended to higher values if the experiments presently being carried out indicate that this technique is effective in enhancing the radiation levels [10].

The pumping system must exhaust the 2 Pa m^3 s^{-1} of He produced by 1.5 GW of fusion power and keep the ambient central helium concentration below 10%. All measurements of helium transport in the main plasma of present experiments indicate that the helium confinement is roughly the same as that of the background plasma for all regimes except the reversed shear regime where JT-60/U reports very long central confinement times for helium. The helium concentration will therefore be similar in the plasma edge and plasma core. However, the helium concentration in present experiments is observed to be lower in the neutral gas in the divertor than in the core of the main plasma by a factor of up to 5 [29]. Thus 50 Pa m^3

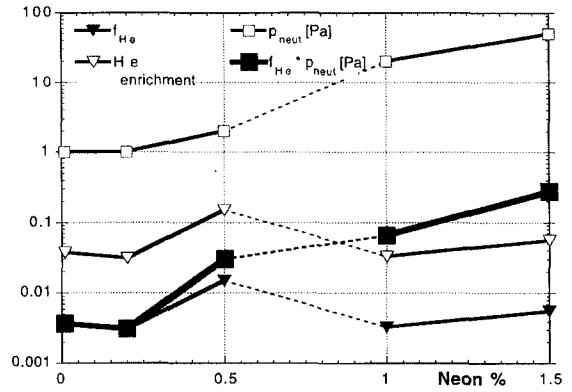

Fig. 10. Neutral pressure helium fraction, helium enrichment and an estimate of the helium partial pressure in the private flux region as a function of the neon concentration at the core-edge interface [23].

s^{-1} of gas needs to be exhausted from the divertor. Thus a gas pressure of 0.25 Pa or greater is needed to ensure He exhaust. Pressures of this magnitude and greater are commonly found on divertor experiments, particularly in highly baffled divertor experiments [30].

He 'de-enrichment' is also found in modelling studies [31]. Studies using the B2/EIRENE and UEDGE codes indicate that the ion thermal force in combination with flow reversal of the background plasma can reduce the helium exhaust efficiency for the ITER divertor configuration [23]. These effects produce a 'flow reversal' in the helium ions. The helium ions circulate in the SOL between the target plates and the main plasma, flowing toward the main plasma near the separatrix and toward the divertor plate further out in the separatrix. This leads to depletion of the helium density near the separatrix [31] and to a concentration of the helium density further out in the scrape-off layer. The pumping in the ITER vertical target divertor is from the private flux region. To reach the pumps, the recycling helium atoms must traverse the plasma near the separatrix. If the temperature of the plasma near the separatrix is above 6–8 eV, most of them will be ionized, resulting in very low helium concentrations in the pump duct. The B2/EIRENE calculations for ITER described earlier indicate that the helium 'enrichment' is 0.04 for a strongly attached plasma (Fig. 10). Additionally, the high temperature along the separatrix for attached plasmas leads to significant pumping of the neutrals in the private flux region, so that the neutral pressure in private flux region is also lower than with detached plasmas which have a significantly higher 'albedo' for the neutrals. This effect has been seen on Alcator C-Mod [13]. The calculated enrichment for ITER with 0.5% Ne is about 0.15. The estimated helium partial pressure ranges from 0.03 to 0.07 Pa, which is adequate for helium exhaust.

The results from present experiments and their extrapolation to ITER have led to the development of the present concept for the ITER divertor. These results and physics design analysis indicate that a variety of atomic processes will be able to spread out most of the heating power over the walls leading to acceptably low peak heat fluxes on the divertor plates. These results also highlight issues needing further research and development including the need to demonstrate the ability to control the level and location of the radiation losses while maintaining adequate core plasma performance, the need to control the helium and impurity transport in the main plasma and divertor and to be able to compensate for transport effects such as the thermal force and plasma circulation in the scrape-off layer. The ongoing experimental and theoretical international research pro-

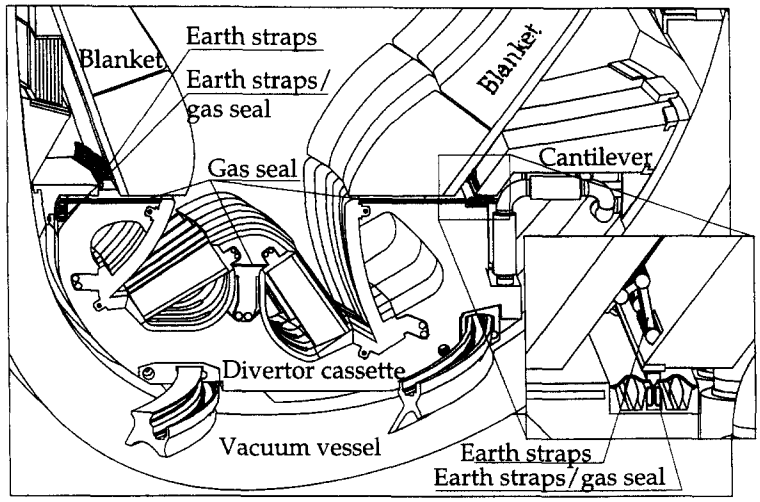

Fig. 11. Divertor cassettes mounted on rails in bottom of vacuum vessel. Insert shows detail of earth-straps connecting backplate to vessel and gas seal isolating divertor from upper chamber.

gram in divertor physics is focused on developing an understanding of divertor operation and methods for reducing the power and particle fluxes on plasma facing components with emphasis on improving the power and particle control system for ITER. The ITER divertor consists of components housed in 60 easily removable cassettes to maximize the flexibility for component repair and modification so that results from this research can be incorporated in the ITER divertor within a few years even after ITER has begun operation.

2.2. Divertor engineering design

The ITER divertor consists of 60 cassettes, each 5 m long and 0.5 m to 1 m wide mounted on toroidal rails which are welded onto the bottom of the vacuum vessel (Fig. 11). The divertor cassette concept has been adopted to serve as a flexible basis for different divertor geometries and at the same time to provide a well defined interface to other machine components and to remote handling. Cassettes located in front of the four dedicated handling ports ('central' cassette) include those containing optical and/or micro-wave diagnostics, while two so-called 'second' cassettes positioned on either side of a central cassette incorporate diagnostic sensors (e.g., magnetics, Langmuir probes, pressure gauges). Six pipes per divertor port route coolant to the cassettes.

The plasma facing components that form the divertor channels for the inner and outer legs of the divertor are supported on a stainless steel cassette body (Fig. 12). This body withstands the electromagnetic forces, provides shielding for the vacuum vessel and coils, and incorporates internal coolant routes which cool the cassette body and act as manifolds for the PFC's. The cassette body can accommodate differing divertor configurations that might need to be tested during the BPP of ITER. It is anticipated that up to three complete replacements of the divertor PFC's will be carried out during the BPP, because of armor erosion and possibly because of changes in the divertor configuration. However, it is foreseen to re-use the cassette bodies for the entire BPP (and possibly EPP),

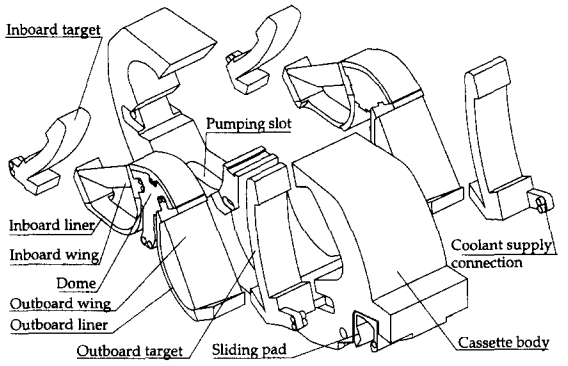

Fig. 12. Exploded view of divertor cassette showing detachable high-heat-flux components.

minimizing both costs and the amount of irradiated waste produced. The replacement of the PFC's is performed more efficiently ex-vessel in a hot cell, where the refurbishment of 60 spent cassettes will take about one year. Therefore a second set of divertor cassettes will be stored in the hot cell in order to facilitate fast replacement (< 6 month) of the spent ones.

The geometry being developed for the first ITER divertor is the vertical target option. In this option a vertical target intercepts the plasma outboard of the separatrix at a poloidally acute angle. The target comprises a stainless steel water cooled structure capable of sustaining the electromagnetic forces, onto which a water cooled (swirl flow) copper heat sink is mounted. The copper is clad with tungsten at the upstream end of the divertor channel in order to minimize erosion and carbon at the downstream end where the highest heat flux is anticipated. A water cooled copper wing [32] mounted in front of a water cooled copper liner (both clad with tungsten armor) protects the stainless steel cassette body at the other side of the divertor channel (in the private region). Finally a dome, which is a water cooled copper structure clad with either tungsten or beryllium, is located beneath the X-point (Fig. 11). It provides a baffle preventing neutrals from entering the main plasma at the X-point and protects the wings from direct interaction with the plasma. It should be noted that the modular nature of the components is an important feature of the design, allowing the PFC's clad with beryllium, tungsten or carbon to be manufactured and fully tested prior to being installed on the cassette body towards the end of the manufacturing cycle.

Targets on adjacent cassettes must be aligned accurately with respect to one another and angled slightly so as to shield leading edges of the adjacent components from direct incidence of the field lines (saw-toothing). However, because the divertor intersects only open field lines, the overall alignment of the divertor against the toroidal field is much less critical than for limiter and baffle modules (± 3 mm). A moderate global misalignment would thus only influence the location of the strike zones on the vertical targets ($> \pm 10$ mm is allowable). Therefore only the alignment between adjacent cassettes and the protection of leading edges is critical in the divertor. The angling which provides this protection has to be as small as possible since it increases the peak heat flux on the already highly loaded vertical targets. A maximum step in the poloidal direction of 2 to 4 mm is therefore under consideration. Costs and manufacturing as well as installation feasibility will determine the final value. In order to achieve an installed tolerance of this order (± 1 mm to ± 2 mm), the toroidal rails onto which the cassettes are mounted, are welded to the floor of the vacuum vessel and then surveyed. The cassette shoes which lock the cassette bodies onto these rails are each accurately machined to suit and the PFC's are rigidly held on the cassette body against machined reference surfaces.

It is predicted that the heat-flux incident on the PFC's when averaged over the surface will be less than 1 MW/m^2 However the design anticipates an uneven power distribution with steady state peak power densities of up to 5 MW/m^2 and transients incident on the highly inclined vertical targets of up to 20 MW/m^2. These high heat loads and the embrittlement of Cu alloys at low temperatures (120°C) by neutron irradiation require to find a compromise between the operating temperature window for the irradiated copper alloy, the optimization of the thermal-hydraulic performance of the PFC's and the size and costs of the divertor heat transfer system (which approaches the costs of the divertor components themselves). Therefore the coolant parameters adopted for the divertor HTS are: 140°C inlet temperature, 4 m^3/s total flow rate, 4 MPa inlet pressure, and 1.5 MPa pressure drop. Testing performed by the CEA at the Le Creusot test facility [33], using the ITER coolant parameters, indicates that a critical heat flux limit (CHF) > 25 MW/m^2 can be achieved.

A vigorous R&D program is in place in the four home teams developing joining techniques suitable for attaching the three candidate armors to the copper heat sink. Highlights in the joining include the progress made in the US using graded copper–tungsten layers and in the EU the use of active metal casting of copper onto carbon and tungsten (the cast Cu can then be welded to a Cu heat sink). The attachment of beryllium to copper is focused on silver free brazing and diffusion bonding using aluminum and titanium as diffusion barriers (inhibits the formation of brittle intermetallics). Repair of damaged beryllium surfaces using plasma spraying is also proving very promising. Beside the three armor materials, three copper alloys for the heat sinks are being investigated by the HT's. These are dispersion strengthened copper, and the precipitation hardenable alloys of CuCrZr and CuNiBe. A final decision on the armor and the heat sink materials, as well as on the joining technique(s) to be used for the first ITER divertor is scheduled for 1998.

For the ITER in-vessel components earth straps are required in the poloidal direction to prevent component damage by arcs and to bypass the current which would otherwise partly flow along the divertor cooling pipes causing them to be damaged by the $J \times B$ forces. The maximum halo current which can occur in one of the divertor cassettes is 200 kA (see also Section 2.3). Thus earth straps capable of conducting such a current are needed between the bottom of the blanket backplate and the divertor cassettes as well as between the blanket/divertor cassettes and the vessel. In addition, gas seals are required at the same location to prevent the relatively high pressure neutral gas in the divertor area from streaming behind the blanket and between blanket modules into the main plasma chamber (Fig. 11). For the same reason the baffle modules follow the 6 cm flux surface and thus support plasma plugging of neutrals in the divertor. High neutral pressure (high neutral flux) around the main plasma would degrade the confinement [34] and increase the tritium take-up in the first wall. From these considerations an allowable gas leak of ~ 30 Pa m^3 s^{-1} (8×10^{21} particles/s) has been specified. The total acceptable gap between divertor and main chamber is then approximately 0.045 m^2 (implying a 0.5 mm gap between the blanket and divertor) when considering sonic gas velocity. Hence beside the opening between blanket and vacuum vessel, the 30 mm gap between the divertor and the baffle and also the 10 mm vertical slot between adjacent cassettes needs to be closed (Fig. 11).

This is achieved with combined gas seals and earth-straps installed between the divertor cassettes and a cantilever structure which is mounted on the vacuum vessel (inboard and outboard) and which is capable of sustaining the electromagnetic loads (Fig. 11). The seal/earth-strap between the cantilever and the divertor cassettes satisfies the gas sealing requirement, acts as an earth-strap, sustains the electromagnetic loads, accommodates misalignment and relative motion during operation and allows a simple remote detachment during cassette removal/installation. In the outboard cantilever additional shielding could be provided to reduce the streaming of thermal neutrons into the divertor port and thus decrease the irradiation of diagnostic equipment and cryopumps. The current path from the blanket back plate to the cantilever is provided through hinged plates with spring washers. The design allows for radial and vertical relative travel of the blanket (~ 6 cm) as well as for a few degrees of rotation. The gaps (vertical) between adjacent divertor cassettes are closed by special ceramic inserts with spring plates.

2.3. Disruption loads

The main causes of large dynamic electromagnetic loads in the divertor are related to: (a) the fast toroidal flux change during a thermal quench at the beginning of a plasma disruption (B_p drops to 0); (b) the poloidal flux change related to the current quench phase, and (c) to the transfer of part of the toroidal plasma current from the plasma halo to the divertor structure. The change of the toroidal flux (a) induces a poloidal current of up to 5 MA in the plasma facing components for the worst cases (high initial β). The time scale of this phenomenon is expected to be about 1 ms, therefore the current tends to flow in a very narrow shell on the surface of the components and has a quite uniform toroidal distribution. The effect of this current is to pull the divertor towards the plasma (maximum force is ~ 1.6 MN per cassette) and to produce a pulling pressure on the vertical targets (about 1 MPa and 0.6 MPa at the inner and outer target, respectively).

The toroidal plasma current decay (b) produces a fast variation of the poloidal magnetic flux in a time scale of the order of 10–100 ms. In toroidally connected structures such as the first wall and back-plate, or the vacuum vessel, the induced current tends to flow in the toroidal direction.

However, in the divertor the patterns of the eddy currents are more complicated and depend upon the connection of the different sub-component to the cassette body. In the wings the eddy current distribution can be regarded as the sum of two loops: one formed by the two adjacent wings on each cassette, the dome at the top, and the cassette body at the bottom. The other loop occurs within each wing itself. The resultant distribution is an approximately linear profile of current which peaks at the wing's edge near the side wall of the cassette and has a smaller peak of opposite sign at the other edge. In the dome surface facing the plasma the current flows almost entirely in the toroidal direction. Since the domes are not toroidally connected, the loop closes through the wings and through the side-wall of the dome support. The magnitude of current and related forces depends upon the current quench duration and the plasma position at the start of the disruption.

Two main cases have been analyzed: a plasma disruption in the equilibrium position (centered disruption, type 1) and a vertical displacement event (VDE, type 2 or 3) followed by a plasma disruption. In the first case, the relatively large distance between divertor and current centroid (about 5 m) reduces the electromagnetic coupling and thus limits the induced current and consequent forces. For the VDE, the plasma would shift slowly (in the time-scale of seconds) toward the null-point and after having interacted with the first wall disrupt in a time scale of several 100 ms. This event was simulated by the axisymmetric TSC code and the time-history and spatial profiles of the plasma current from these calculations were then used in more detailed 3D codes to calculate the eddy currents and forces. The simulation produced a VDE with a maximum downward displacement of the plasma of 4 m in about 5 s and a current quench phase duration of 300 ms. The eddy currents induced in the divertor reach 13 MA m^{-2} (edge of the inner wing) causing a peak pressure normal to the wing surface of about 3.5 MPa at the outer channel. In the inner channel the peak pressure is about 2.5 MPa. Because of the relatively slow current quench phase the current diffuses through the whole thickness of the copper based PFC's, and relatively large currents flow also in the rear part of the cassette body. Prior to the current quench, the plasma comes in contact with the first wall and a halo current flows in the poloidal direction between the outer and inner wall. The important parameter for the design of the divertor is the product of halo magnitude times the peaking factor, as this determines the maximum current in one divertor cassette. In the case analyzed, the halo current reached 29% of the initial plasma current and a toroidal peaking factor of 2 was assumed. The maximum current in the cassette is then estimated to be 200 kA. The time evolution of this current is related to the plasma current quench phase, with the peak current reached half way through the current quench following the VDE.

From the structural point of view the toroidal current quench after a VDE and the halo currents produce the most demanding loading conditions. The loads caused by the toroidal flux change (a), although similar in magnitude to case (c), have a much smaller impulse because of their short duration, since the inertia of the structure reduces significantly the impact of these loads. In case (b) the present configuration of the wing appears not adequate to sustain the large pressure. The bending stress estimated for the present design of the wing (60 mm thick) is 350 MPa, approaching the elastic limit of the unirradiated Cu alloy (the yield stress at 300°C is about 380 MPa). The overall effect on the cassette body is a twisting moment of 1.5 MN m around a vertical axis, which produces a reaction force of ~ 0.5 MN in toroidal direction at the rail. The stresses in the cassette body produced during the VDE by halo currents (c) have been estimated with static calculations. The bending stress peaks at 250 MPa near the inner support of the cassette. This stress exceeds the allowable for normal operation conditions and frequent transients but would not cause plastic deformation of the structure. In addition some local plastic deformation of the divertor structure is deemed as acceptable for this sort of unlikely event. In any event, the stress can be reduced by either thickening the cassette cross-section where the maximum stress occurs, or by reducing the current in the cassette by providing a lower resistance path to the vessel. More accurate modelling calculations and further design optimization is required to reduce the stresses in the wings.

2.4. Divertor maintenance

Due to the fact that the divertor in ITER is expected to be replaced relatively frequently (3 times during BPP) a fast and reliable remote handling scheme for divertor maintenance is required. To this end 4 dedicated ports were allocated to allow remote handling of the divertor cassettes. The goal is to perform the replacement of a complete divertor in less than 6 months (parallel operation on all four ports) and to exchange a single cassette centrally located between two handling ports (worst case) within 2 months.

The cassette concept with 60 segments appears well-suited to the task of expediting divertor maintenance. Of the 15 cassettes installed through a given handling port, 12 are standard cassettes, two are so-called 'second' cassettes positioned on either side of a 'central' cassette located directly in front of the handling port. During cassette installation/removal remote handling casks provide containment while transporting the cassettes as well as other components (e.g., cryostat closure plate, in vessel remote-handling (RH) tools) between the hot cell and the divertor level at the ITER machine (Fig. 13). All the casks dock through a double door mechanism to one of the 4 divertor remote handling ports. In order to gain access to the cassettes the cryostat closure plate, the bioshield plug and the vacuum vessel flange must be removed by special tools operating from inside a remote handling cask. For cassette

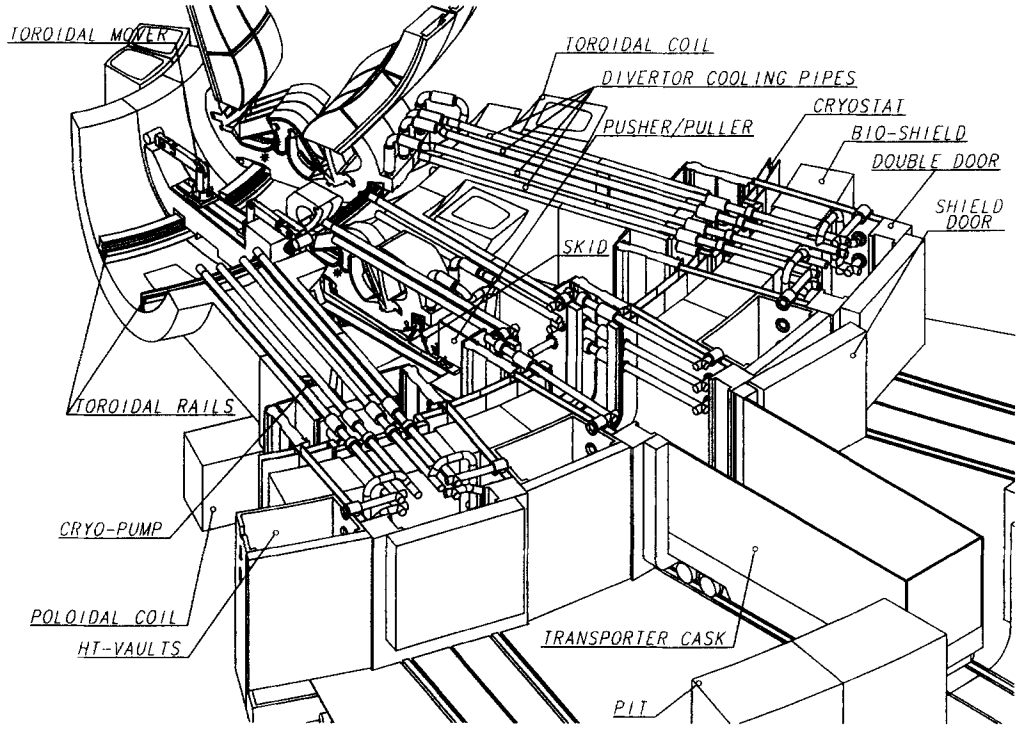

Fig. 13. Cutaway view showing divertor maintenance in progress. A cassette is being moved out of the machine to a remote handling cask.

installation a radial mover pushes the cassette which is mounted on a skid from the cask along radial rails through the handling port into the vessel (Fig. 13). Inside the vessel a toroidal mover inserts forks beneath the cassette, lifts and transports the cassette around a pair of toroidal rails to its designated position. Once at its final position the cassette is locked to the toroidal rails by wedges (operated by a ball-screw mechanism) in such a way that it can sustain

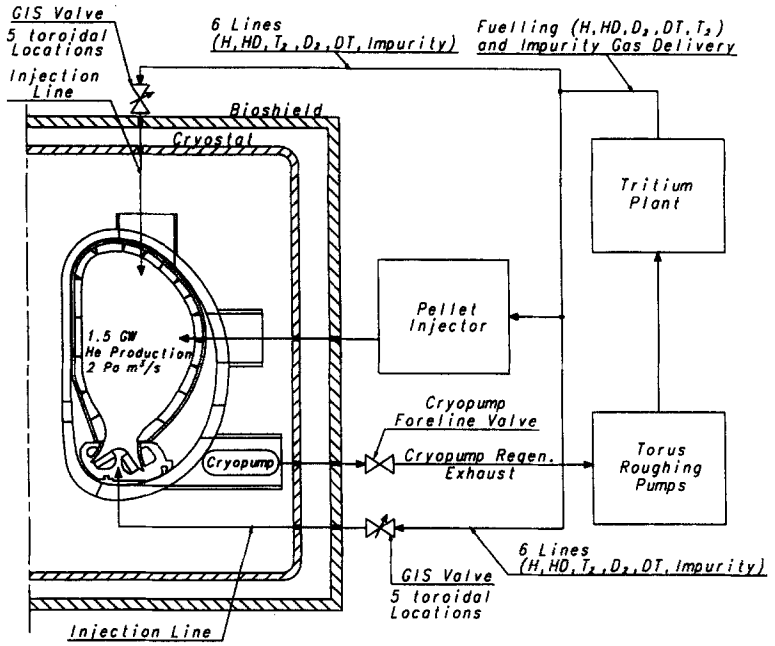

Fig. 14. Schematic of the gas and pellet fuelling systems, primary and secondary pumps, and tritium plant.

the disruption loads and at the same time is accurately aligned-in both poloidal and toroidal directions. The above mentioned second and central cassettes are installed by special skids performing similar operations as described above.

Another remote handling operation taking place in parallel to the cassette installation is the cutting and welding of the divertor cooling pipes. This operation is performed by a special remote handling cask which docks to every port, opens the cups on the pipe ends extending from the closure plate, inserts a crawler with a cutting/welding tool and then cuts/welds the pipes close to the cassettes approximately 10 m downstream of the pipe ends.

2.5. Pumping and fuelling

The pumping and fuelling system must: provide the throughput of DT required for ignited operation; remove helium from the plasma exhaust at the rate it is produced and at core levels low enough to permit sustained burn; and provide seed impurities for divertor heat flux control (see Section 2.1). The minimum required total gas

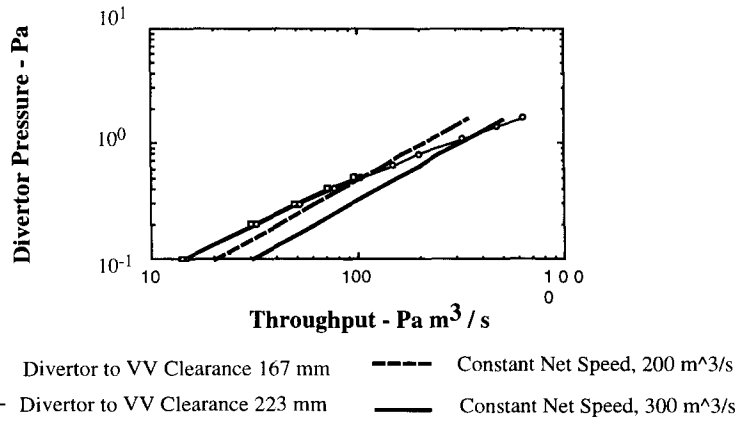

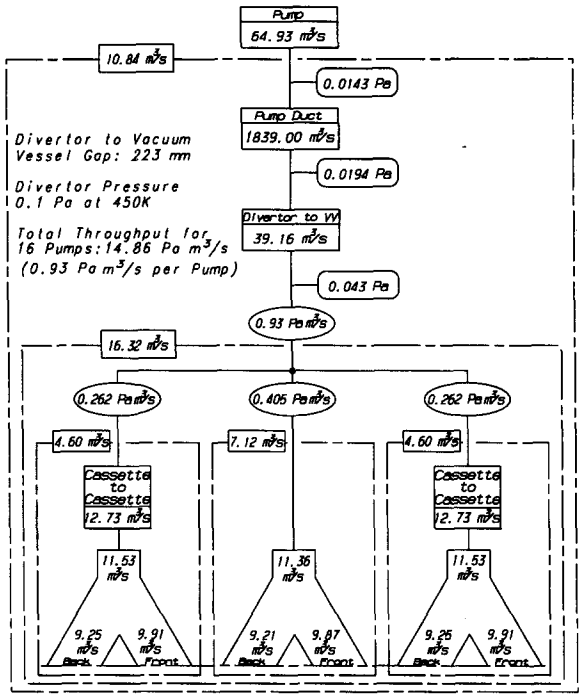

Fig. 15. Pumping throughput characteristics of cassettes and pumping system. Lower: Conductances of pumping slots and pathways to tie pump for a group of 3 cassettes (1 port). Also indicated is the throughput at 0.1 Pa divertor pressure. Upper: Divertor pressure versus throughput indicating increase of pumping speed in transition regime.

throughput (H_2, D_2 and T_2) for He exhaust is ~ 50 Pa m^3/s when assuming a He concentration of 10% in the main plasma and a He enrichment factor of ~ 0.2 in the divertor. However, for operation modes where a SOL flow will be generated to promote impurity retention, an increased throughput is required and up to 200 Pa m^3/s steady state is currently specified. Also, for start up and fast control actions up to 500 Pa m^3/s is the present design requirement. These plasma physics based requirements are the design drivers for the fuelling system, for the pumping system and for the T-plant which has to clean impurities from the exhaust gas and to separate the hydrogenic isotopes.

The fuelling system consists of a gas and pellet injection systems. The gas injection system is composed of six fuelling lines (DT, T, D, and 3 impurity lines, e.g., N_2, Ne, and Ar) and a pumping/flushing line, all mounted inside a vacuum pipe to provide secondary containment. This fuel line assembly is routed from the tritium plant to two ring manifolds, one on top of the machine and the other at the divertor level (Fig. 14). Each ring manifold serves 5 injection points distributed toroidally around the machine. The dosing valves, at each injection point, are mounted inside vacuum sealed and magnetically shielded valve boxes located outside the bioshield. The valves are connected to the plasma/divertor volume through one common delivery line, 15 to 20 m long and 10 mm diameter, at each location.

A design study was recently completed to size the pipes for the gas injection system and to analyze the gas-flow response to various types of transient conditions. Thus a simplified model for the analysis of the gas flow through pipes has been developed [35]. Typical response times calculated when changing the gas flow with the dosing valves are ~ 100 to 200 ms considering 0.1 MPa pressure in the manifolds. The diameter of the manifold lines serving the valve boxes have been sized to supply 500 Pa m^3/s for 50 s (equivalent to steady state) resulting in 2 to 3 cm diameter for the D, DT and H/He and 1 cm for all other lines. The T inventory in the gas injection system was estimated to be ~ 15 g.

In addition to the gas injection system two centrifuge pellet injectors are installed in a transport cask at the midplane with their flight tubes routed through a midplane port. The cask provides secondary containment and allows rapid removal of the injectors for off-line maintenance. Each injector has 3 extruders of which one is producing pellets, one is making ice and one is in standby mode. Only one of the two injectors is active at a given time launching 6 to 8 mm pellets with a speed up to 1.5 km/s. The pellets penetrate up to 20% of the minor radius and thus might pass the ELM effected area. Each injector is designed for a fuelling rate of 50 Pa m^3/s with pure T_2 pellets and 100 Pa m^3/s for other hydrogenic species. The tritium inventory in the pellet injectors is ~ 65 g.

The 50 Pa m^3/s T fuelling capability of the pellet injectors and a similar capability of the T plant for steady state isotopic separation of D and T allows to apply a fuelling mode labelled 'isotopic tailoring'. In this mode the pellet injector is used to deep fuel T while up to 150 Pa m^3/s of D_2 is introduced by gas puffing. Calculations show that with the above stated penetration a reduction of the T content in the SOL by factor 2 can be achieved while retaining a D–T ratio of $\sim 50\%$ in the main plasma [36]. This mode therefore allows to reduce the T impinging onto the first wall by factor 2 and thus the T inventory stored there (see Section 4.4).

The primary pumping system in ITER consists of two major subsystems, the torus roughing system and the torus high vacuum system. The torus roughing system is designed to perform two primary functions: evacuation of the torus to < 50 Pa from atmosphere in less than 60 h with the torus back filled with air, helium or nitrogen; and to regenerate the primary cryopumps to $< 5\%$ of their initial inventory in < 62.5 s during the plasma burn.

The torus high vacuum pumping system consists of sixteen (16) batch regenerating cryopumps, located in the divertor ports. The pumps are provided with inlet valves which are used to throttle the exhaust flow for particle control in the case of high neutral pressure in the divertor (> 1 Pa). In order to keep the T inventory on the pumps to < 140 g, every 62.5 s a pump starts regenerating for ~ 250 s. With 12 pumps in pumping mode while 4 are in regeneration a gross pumping speed of 1,000 m^3/s is achieved. However, limited conductance through the divertor pumping slots (175×375 mm) and through the 200 mm clearance between the underside of the divertor cassette and the vacuum vessel results in a net pumping speed of ~ 200 m^3/s being available in the divertor private region (Fig. 15). This pumping speed implies that 0.3 Pa and 0.8 Pa neutral pressure are required in the divertor private region to achieve 50 Pa m^3/s and 200 Pa m^3/s, respectively. These neutral pressures are readily achieved in present day machines during detached or semi-detached divertor operation [37].

3. First-wall and shield design

3.1. Design description

The design concept for the first-wall and shield is shown in Fig. 16 [38]. Although some details having to do with segmentation, manifold layout and attachment (see discussion below) are still being finalized, the approach of fabricating the first-wall and shield as a set of mechanically monolithic modules of rough dimensions $1 \times 2 \times 0.3$ m^3 is fixed. In comparison to the poloidally modular concept of the outline design, the present concept has a far more robust first wall and mechanical structure, is more easily fabricated, and most importantly lends itself to less complex remote handling operations thereby reducing the time required for repair or replacement.

The majority of the modules have a first wall which consists of a copper-alloy mat (DS or CuCrZr) in which are imbedded 10 mm OD, 1 mm wall, stainless steel cooling tubes. The Cu mat is bonded to the shield block which is formed from 316 LN SS and has internal cooling passages to remove the neutron generated heat. Beryllium tiles or a castellated beryllium mat is bonded to the copper and thus Be is the predominant plasma facing material. In addition to these 'primary wall' modules, a set of baffle modules, located just above the inner and outer vertical targets of the divertor, and a set of limiter modules located between the outer baffle module and the horizontal port (See Fig. 1) complete the first wall. The basic configuration for all modules is the same; however, the baffle and limiter modules have copper pipes with a thin (0.2 mm) SS insert in order to increase the permissible heat flux to 3

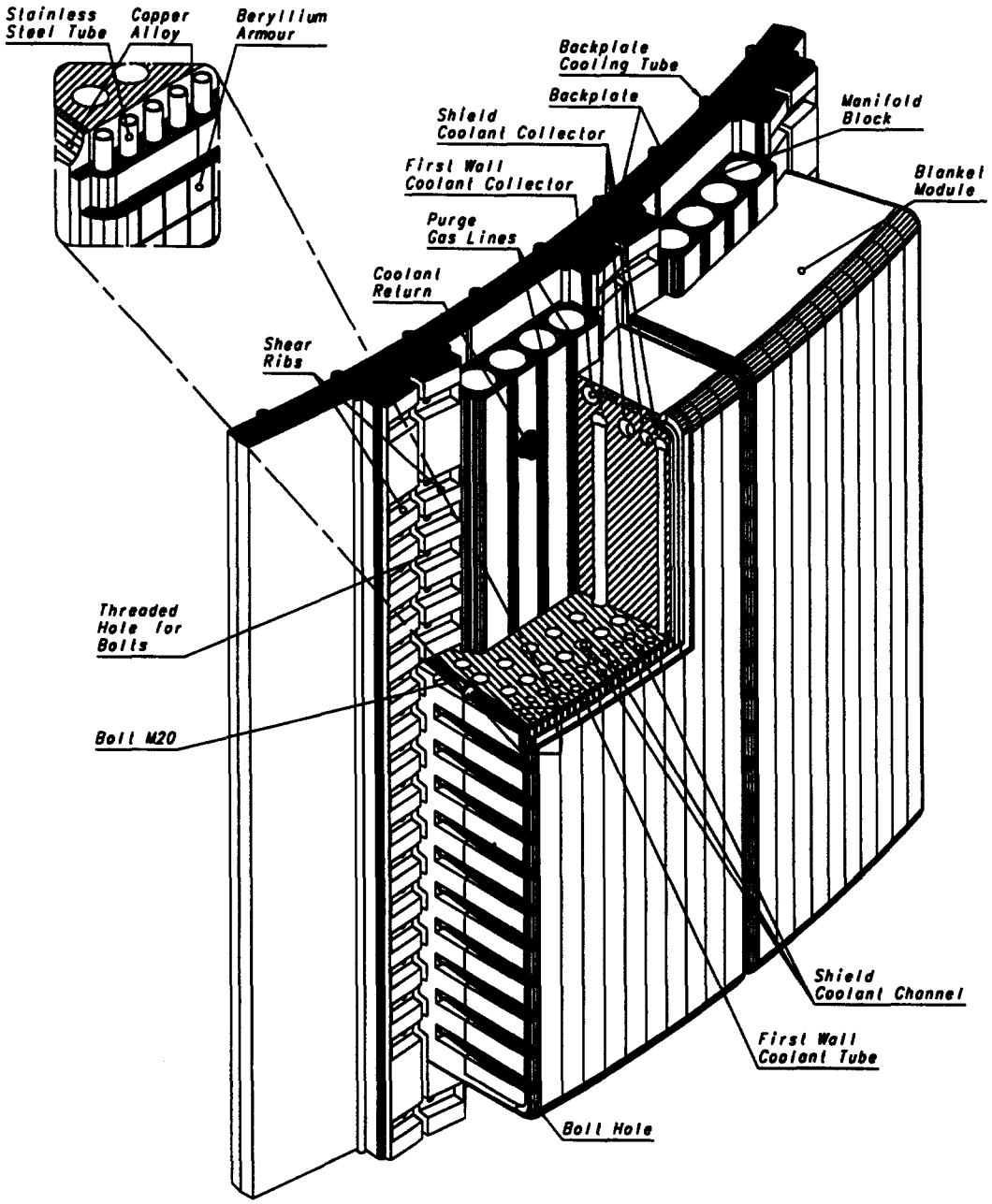

Fig. 16. Cutaway view of the first-wall/shield module located at the inside mid-plane. A mechanical attachment to the backplate is shown. Other variants of the method of mechanical attachment, as well as a welded attachment, are under consideration.

and 5 MW/m^2 respectively. The limiter, whose PFM is also Be, provides the surface for plasma start-up and shutdown during periods when it is not possible to form a diverted configuration. The baffle is aligned to the flux-surface passing 6 cm outside the separatrix at the point of minimum scrape-off width, and serves to prevent neutrals from streaming from the divertor region to the main plasma. The lower third of the baffle's first wall is tungsten which, owing to its high sputtering threshold, results in maximum baffle lifetime. While several fabrication and bonding methods for the first-wall/shield modules are being developed in the R&D program, methods employing hot isostatic pressing (HIP) appear particularly well suited to the design.

The heat removal capacity of the first wall and module is consistent with a spatially peaked neutron wall loading of 1.2 MW/m^2 and a surface plasma heat flux of 0.5 MW/m^2. At the representative operating point whose parameters are given in Table 1, the average heat flux to the wall from bremsstrahlung would be approximately 0.1 MW/m^2, corresponding to a total power of 100 MW. Thus the first wall design has considerable margin with respect to this nominal value, and such margin provides the flexibility to accommodate either high peaking factors, as might arise in the case of a MARFE, or a larger fraction of radiated power to the first wall as would result from higher intrinsic or seeded impurity levels.

3.2. Disruption loads — mechanical

While the modular shield design is a particularly robust solution to the FW/shield design problem, it is recognized that occasional changeout of modules as a result of disruption damage or component failure will be required. It is then necessary to be able to remotely detach the module from the backplate and install a new or repaired module, and to accomplish this task, which includes also disconnecting and connecting the module to the manifolds carrying the cooling water, in as short a time as possible. A key issue in this remote-handling operation is then the method by which the module is attached to the backplate. Since this connection is highly stressed by the effect of disruption forces, the problem of its design turns out to be the most challenging of all those arising in connection with the design of in-vessel components.

Two basic approaches are being considered, one based on welding and the other mechanical, i.e., using bolts or studs. The concept illustrated in Fig. 16 is an example of a mechanical attachment; however variants on the approach illustrated here are also being explored. The present situation is that both welded and mechanical attachment can satisfy the design requirements and the decision between the two approaches, which will be made for the Detailed Design Report due later this year, will be made mainly on the basis of minimizing the downtime required for replacement.

An appreciation of the problem can be gained from examining the results of the analysis of the welded option which is similar to that shown in Fig. 16, except that the module is attached to the backplate by a continuous weld which replaces the keys or 'shear-ribs'. In a type 1 disruption, which gives rise to the most severe loads on the attachment, the plasma toroidal current is largely transferred to the first wall resulting in a surface current density of about 1 MA/m flowing on the surface of the modules located near the midplane on the inside of the torus. As illustrated in Fig. 17(a), the effect of this current is (1) to produce a traction on the surface of the module, amounting

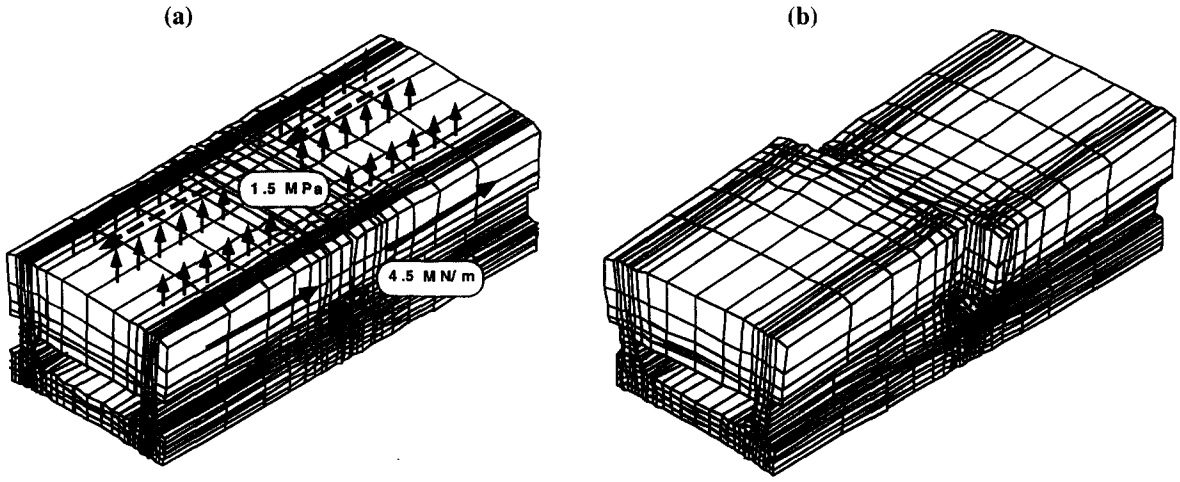

Fig. 17. (a) Finite element model and loads used in analysis of first-wall/shield module response to type 1 disruptions. The module is located at the inside mid-plane of the machine and a welded attachment to the backplate is considered. (b) The distortion of the backplatemodule system arising from the loads in (a). The maximum displacement is 1.5 mm.

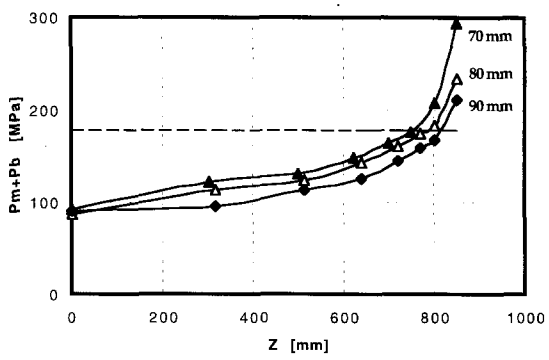

Fig. 18. Maximum membrane plus bending stress in attachment leg resulting from the module and loads defined in Fig. 17. The coordinate z measures distance along the leg from the module midplane. The curve labeled 1.5 S_m corresponds to the allowable for 316 LN at room temperature. For a 90 mm thick leg, the stress is within the allowable except at the ends where the localization of the peak stress is sufficient to be acceptable.

to an average value of 1.2 MPa (design value 1.5 MPa); and, since it must cross the toroidal field on the sides of the module, (2) to produce equal and opposite poloidally directed forces on the sides of the module of about 4.5 MN/m. These forces form a couple which tends to twist the module as shown by the deformed shape in Fig. 17(b). Of paramount interest are the stresses in the support leg which are shown in Fig. 18, from which it can be seen that the maximum stresses are within allowables for the reference leg thickness of 90 mm for the inboard mid-plane modules.

In the case of type 2 and 3 disruptions (VDE's), the main stresses occur in the backplate rather than in the module or its attachment. In the calculation summarized in Fig. 19, a halo current of 8.4 MA (40% of the initial plasma current) is assumed to flow between the lower modules on the inner and outer sides of the backplate. In addition a toroidal peaking factor of 1.5 is assumed, which means that the peak poloidal current density is 50% higher than the toroidally-averaged value. In this case, the maximum membrane and membrane plus bending stress is found to exceed the allowables for normal operation by about 20%. While this stress level can be considered acceptable for relatively rare events, it is clear that such disruptions produce the bounding cases for backplate design. Thus mitigation of VDE's, for example as has al-

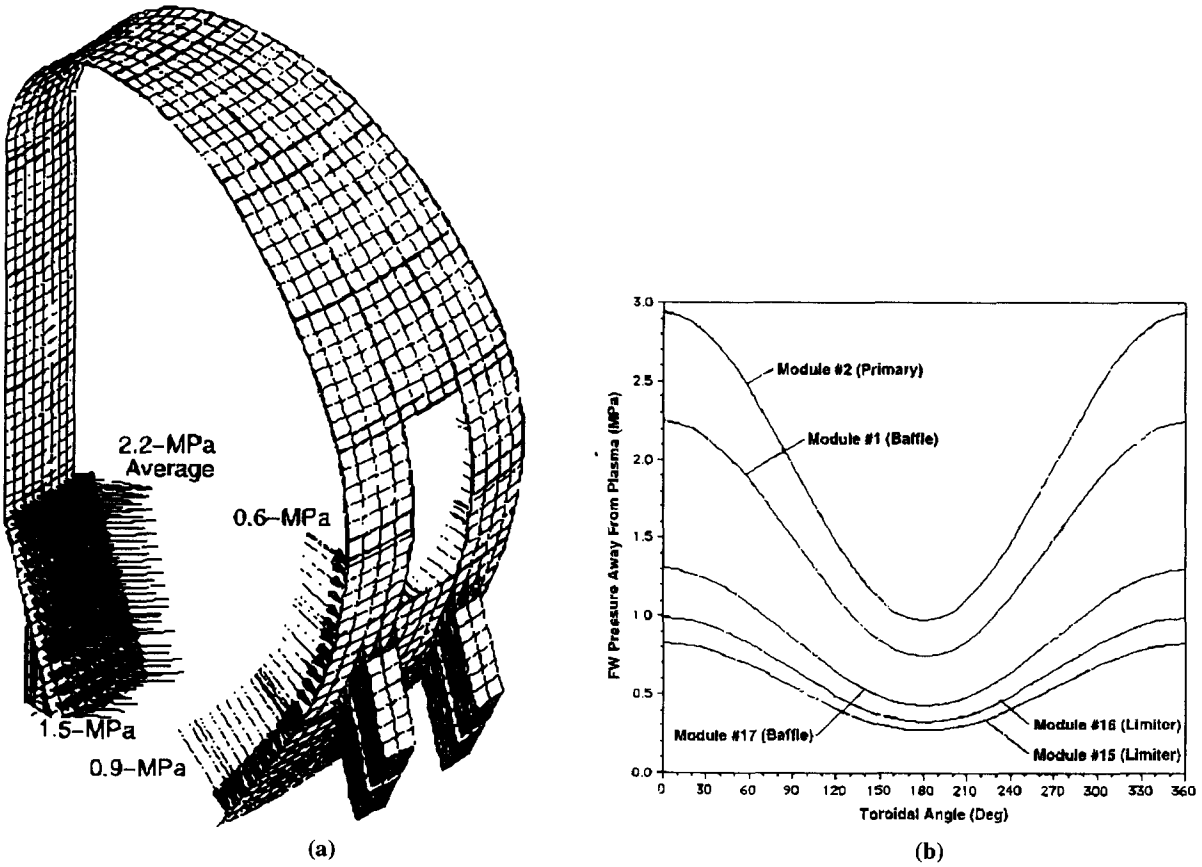

Fig. 19. Model of effects of halo current showing (a) poloidal distribution of pressure on backplate and (b) toroidal variation.

ready been proven successful by injection of 'killer pellets', is a continuing subject of research in the voluntary physics R&D program.

3.3. Disruptions loads — thermal

An additional effect produced by disruptions is a strong plasma–wall interaction in which a fraction of the plasma thermal energy is released to the wall in a relatively short time, typically within a fraction of a second. This effect is expected to be particularly severe for type 3 disruptions in which the plasma can contact the wall while it still contains most of its thermal energy. Estimates indicate that energy densities of 20–60 MJ/m^2 can be released to the wall over times of order one second. In such cases, the rapid release of energy raises the wall temperature to the melting point and subsequent melting, evaporation and possibly vapor shielding partially reduce the energy flux incident on the unmelted zone.

The loss of material occurring in such events, together with the thickness of the wall and the disruption frequency, will then determine the point at which repairs will be needed. The type of repair required could be either adding FW material to areas in which heavy loss of the melt layer has occurred, or changeout of the entire module if the energy transferred to the cooling system is sufficient to cause burnout and consequent destruction of the first wall. In the former case, repair is possible in situ by plasma spray of the first wall material (Be or W). Encouraging results have been obtained in the R&D program for this technology and the possibility of in situ repair for certain in-vessel components in ITER is becoming increasingly viable.

The likelihood of more substantial damage caused by coolant burnout can be mitigated by taking advantage of the first wall thermal inertia [39], which protects the wall for relatively short contact times (< 1 s), and active intervention through the PF coils and/or killer pellets for longer times. The effect of thermal inertia on reaching the critical heat flux is illustrated in Fig. 20. It shows that for a 10 mm thick FW, a disruption depositing 20 MJ/m^2 never causes the critical heat flux to be reached, while for 60 MJ/m^2 burnout conditions are reached only for interactions lasting over 0.5 s by which time some intervention may be possible. Increasing the Be thickness in the regions of strong VDE interaction would further delay the time at which intervention would be necessary. Of course both the interaction time and the energy density are subject to uncertainty, as is the possible beneficial effect of vapor shielding which is not included in this calculation. Work on more accurate modelling of the disruptions and resulting forces, and optimizing the FW design, is continuing.

3.4. FW / shield remote maintenance

Remote maintenance of the FW/Shield is carried out by means of a vehicle which moves on a toroidal rail

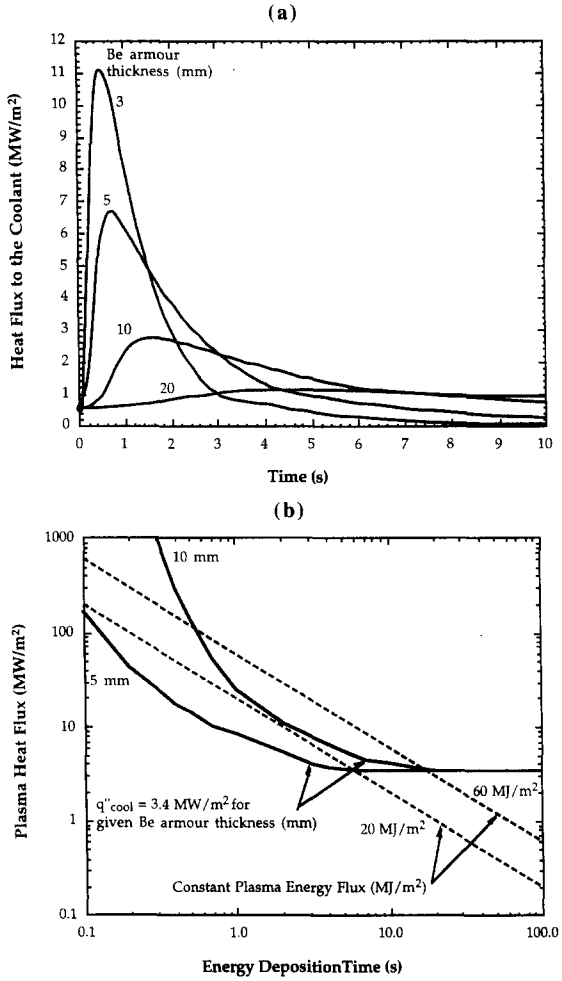

Fig. 20. (a) Heat flux to the first wall coolant from a type 3 disruption in which 60 MJ/m^2 is deposited to the wall during a time of 0.3 s. (b) Transient heat flux to the first wall which results in critical heat flux to the coolant versus heat pulse duration for FW thicknesses of 5 and 10 mm. Also shown are contours of 20 and 60 MJ/m^2 energy deposition [39].

inserted from two of the four dedicated remote-handling mid-plane ports. The vehicle is equipped with an articulated arm which is capable of gripping any of the FW/Shield modules and bringing it into a position suitable for the vehicle to transport it to one of the remaining two RH ports. From there it can be removed and transported to a hot cell where it is repaired or prepared for salvage. Before removal, the cooling connections must be cut by a cutting tool which accesses the connections from inside the cooling manifolds, and the connection to the backplate, which as discussed above could be made either by welding or by a mechanical connection (i.e., bolts or studs) must be cut or unbolted. The project requirements for changeout times are very demanding: 8 weeks for one module, 3 months for a toroidal array of modules and 2 years for all modules. Analysis by the home teams indi-

cates that, although stringent, such times are feasible with the proposed approach.

4. Materials choice for in-vessel components

The choice between the three candidate plasma facing materials (Be, CFC, W3Re) is determined by the expected erosion lifetime, by the capacity to retain tritium, by the local plasma parameters (ion flux, neutral flux and temperature) and power loads as well as by their potential contribution to radiation losses and Z_{eff} in the main plasma. For special locations such as the divertor strike zones and certain areas of the first wall, disruptions and slow high power transients can have a significant impact on the expected erosion lifetimes.

The amount of T retained in the bulk of the plasma facing material depends on the impinging ion/neutral flux, on the surface recombination coefficient for T as well as on the diffusion coefficient and thus on the temperature of the material. In addition neutron induced traps and codeposition of C and T can further enhance the T inventory in the machine. Due to the different nature of plasma wall interaction on different areas of the first wall and divertor, the optimum choice of PFC will depend on the particular location.

4.1. Erosion lifetime of the divertor strike zones

Erosion is due to (a) physical and chemical sputtering, (b) disruption thermal quench and (c) slow transients (for a fuller description see [40] and references therein). Physical sputtering is considered for all three materials (Be, CFC and W3Re) while chemical sputtering is only relevant for CFC. Since tokamak experiments (TS, DITE, ASDEX Upgrade, JET) regularly show lower chemical sputtering at the target than laboratory experiments at low flux, a flux dependence of the yield as $\Gamma^{-0.22}$ was used in the assessment [40]. The power load is assumed to be carried equally by particles and radiation. The lifetime that would result from sputtering processes only would be several 1000 shots for Be, 10000 shots for CFC and very large for W ($\sim 10^5$).

Erosion by a disruption thermal quench is evaluated from published modelling, including the effect of vapor shielding which reduces the energy actually reaching the plate to a few percent. The net evaporation for all materials is included. In addition, metals (Be and W) suffer from surface melting. In the absence of more definite indications, either 10% or 50% of this melt layer is assumed to be lost on average per event. Thus about 30 μm per disruption would be lost for CFC, and between 23 and 75 μm per disruption for Be and W. For the lifetime assessment disruptions are assumed to occur in 10% of the shots.

Slow high power transients represent short (10 s) periods of attached operation for which the power reaching the divertor plates is higher, 20 MW/m^2, than the nominal power of 5 MW/m^2. Such transients are assumed to occur once every 10 shots. Since the thickness of the PFC is determined from a limiting surface temperature (1080 K for Be, 1780 K for CFC and W) at 5 MW/m^2 in order to maximize the lifetime, such transients lead to strong evaporation and, in the case of metals, melting. Because of its low melting point, beryllium is particularly influenced by these transients. It was expected, both from experiment and theory, that the impurities released during such a transient would radiate and thereby limit significantly the melt layer depth (low density vapor shield). However, a

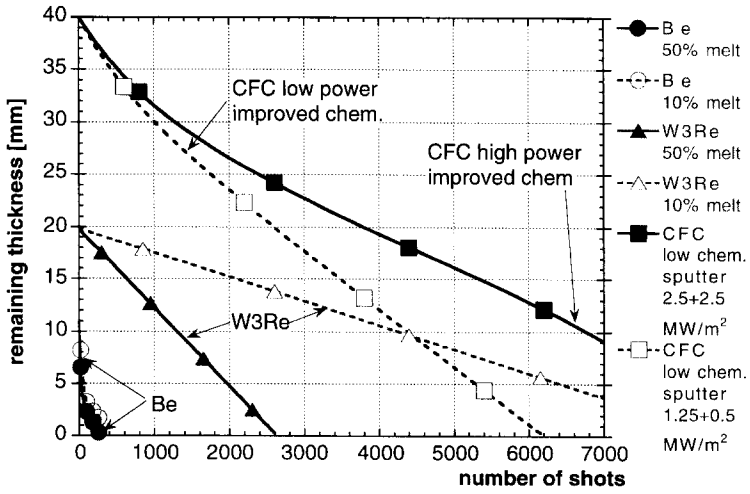

Fig. 21. Remaining thickness versus shots for Be, CFC, and W3Re. Nominal power load during burn 5 MW/m^2. 90% redeposition. Erosion includes physical and chemical (CFC) sputtering, disruption erosion (10% of shots) and erosion by transients (20 MW/m^2 for 10 s once every tenth shot. Initial thickness 11 mm (Be), 20 and 30 mm (W3Re) and 40 mm (CFC). Melt layer loss varied for metals. Improved chemical sputtering only shown for CFC (recommended value, see text). For CFC, two points in power profile considered [40].

recent dedicated experiment on JET [41] showed that less than 5% of the released Be was ionized, little mitigation was observed, strong melting resulted, and 3 mm melt layer was lost in five such events (25% of the expected melt depth per event). Consequently, mitigating impurity radiation is not assumed for further design assessments.

The resulting composite lifetimes are shown in Fig. 21. The Be lifetime is low and dominated by slow transients, which lead to erosion for thicknesses greater than 3 mm. The CFC lifetime is determined by all three processes (transients affect the lifetime only beyond 19 mm, an increase in thickness to 40 mm increases the lifetime by a factor 1.5 to 2). The W3Re lifetime is dominated by disruptions, once the limiting thickness is fixed at 20 mm (transients do not influence the lifetime below this thickness and are very strong above, see Fig. 21, so that an increase of thickness beyond 20 mm is not useful).

For Be, the lifetime is inadequate, 120–320 shots. For W3Re, it is 2400–7700 shots, depending on the melt layer loss, and for CFC it is 5800–8200 shots, depending on the local power because the chemical sputtering yield is temperature dependent (peak at 1000 K).

As a parameter study, the effect on erosion lifetime when designing the ITER divertor for higher power semi-attached (up to 10 MW/m^2) or attached (20 MW/m^2) was investigated [40]. The surface temperature requirement leads to smaller thickness than for fully detached operation; at the same time, sputtering would increase since a larger fraction (less radiation) of the SOL power is carried by particles and the plasma temperature in front of the divertor plate is higher ($\sim$ 20 eV). However, high power transients become relatively less important since the difference between transient and normal operation is then smaller. The results are shown in Fig. 22. The Be lifetime drops below 100 shots. However, more than 2000 shots for CFC, and 1500–4000 shots for W3Re, are still obtained.

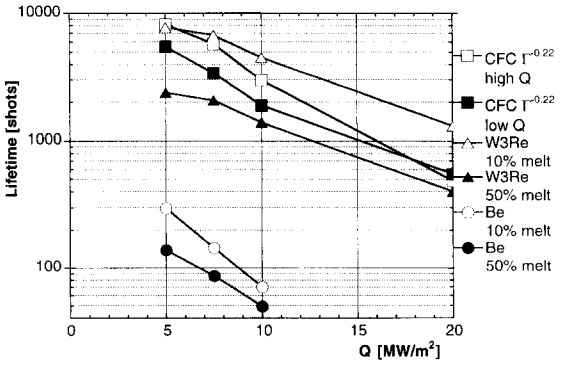

Fig. 22. Erosion lifetime for Be, CFC and W as power is increased from detached to semi-attached operation (Plasma temperature is varied at same time). Thickness determined by max. surface temperature of 1080 K (Be) or 1780 K (W and CFC). Redeposition and erosion processes as in Fig. 21 [40]. For metals, melt.layer loss is varied. For CFC, two points in power profile are considered.

On the basis of this lifetime assessment and because a non-melting material is preferred at the strike zone for initial operation, CFC cladding 3–4 cm thick (depending on CFC type) has been chosen for the lower part of the vertical targets.

4.2. Erosion lifetime of divertor side walls and bottom part of the baffle

The erosion lifetime of the divertor side walls (upper part of vertical target, wings, dome, liner, baffle) is determined by sputtering by neutrals, assumed to carry 0.5 MW/m^2 at average temperatures over 10 eV. Under these conditions, the lifetime ([40], see also chemical sputtering discussion above) is about 1000 shots for Be and several 1000 for CFC, too short for components such as the bottom part of the baffle for which frequent replacement is not planned. In contrast, because of its higher sputtering threshold, W has a lifetime of tens of thousands of shots at least, so that from lifetime considerations tungsten is the material of choice for cladding in this area. (To obtain the actual lifetime, the erosion and surface melting resulting from the reradiated energy during a disruption thermal quench at the target will have to be investigated.)

4.3. Effect of transient loads on startup limiters

Peak power loads on the startup limiters depend crucially on alignment considerations; even rather stringent alignment requirements give heat loads close to 5 MW/m^2 during startup [42]. If the surface temperature is limited to 600°C and with a cooling circuit similar to the one of the blanket (55-liner), the thickness of Be is limited to 5.3 mm. if the ongoing R&D proves that the Be surface temperature is allowed to go to 800°C, then 10 mm thickness would be feasible.

A vertical displacement event can deposit 60 MJ/m^2 within 0.3 to 1 s onto the first wall or the limiter (Section 3.3). This leads to erosion of Be by 0.6 to 1 mm per event, depending on melt layer loss, a value which is 2 to 3 times the erosion per event of a 40 mm thick CFC. Therefore CFC would be the choice from the power loading point of view.

However, chemical sputtering during normal operation and thus the increased plasma pollution as well as enhanced co-deposition of T have to be also considered. An increase of the main plasma Z_{eff} due to C produced on the first wall/limiter would reduce the allowable concentration of a divertor radiator (e.g., Ne, Ar) and thus reduce the ability to radiate the majority of the SOL power before it reaches the target. On the contrary the loss of Be during VDE's is severe, one fifth to one tenth of the thickness per event. Whether the present design choice for the startup limiters, Be, must be replaced by CFC will therefore depend on a judgement on the frequency of these off-normal events (and therefore the success of mitigation mea-

sures), on the impact of CFC (or possibly doped CFC) on the T inventory and on plasma pollution as well as on the severity of the structural damage to the Be per event.

4.4. Tritium inventory in PFC's

Estimates of the tritium inventory and of the permeation through PFC's are important for: the choice of plasma facing material; for predicting the tritium supply requirements; for assessing the radiological hazards from routine operation and from potential accidents; and for the design of the water detritiation system. Unfortunately, quantifying tritium inventory and permeation in PFC's is still subject to large uncertainties which are mainly associated with: the predicted plasma parameters in the SOL (heat loads, particle fluxes and energies), the characteristic tritium-transport related material properties (i.e., diffusion coefficient, rate of surface recombination), the radiation damage related effects (i.e., density of n-induced traps) and the design features of the PFC's (i.e., type and thickness of plasma facing materials, replacement schedule for sacrificial components).

A study was recently conducted to estimate the impact of the above uncertainties on the T inventory and permeation in ITER [43,1,44]. It included the mechanisms of implantation, recombinative surface desorption, bulk diffusion, trapping at neutron induced traps, tritium generated by neutron transmutation in beryllium and codeposition. Three parameters were found to have the greatest impact on this study: (1) the Be-surface recombination rate coefficient [45], (2) the particle flux impinging onto the wall, and (3) the density of n-induced trap sites. Ongoing R&D is expected to narrow some of the existing uncertainties in this area. As far as the Be surface recombination coefficient is concerned, we bracketed the value recommended by Andrew et al. [45] up and down by a factor of 10. However, even though preliminary and awaiting further experimental confirmation, some new experimental results on tritium implantation in beryllium are becoming available [46] and contrary to the original expectation, recombinative desorption of implanted hydrogen ions at high fluxes seems to be largely enhanced due to the increase of the exchange surface area resulting from micro damage. The implanted hydrogen is found to collect in bubbles, eventually growing to form interconnected porosities opening to the surface. Once such porosities open, there is virtually no more uptake of hydrogen. Implanted ions very quickly find a free surface where they recombine and return to the plasma. This in turn could result in much higher recombination coefficients than those indicated in Ref. [46] which provided the basis for the values assumed in this study and in turn in a substantially reduced net flux of tritium atoms migrating into the bulk. However, exposure to lower fluxes (representative of the first wall of ITER), in addition to effects resulting from mixing of materials and the contamination of the Be surfaces with C and O remain to be carefully investigated.

In Refs. [43,44] the tritium inventory in the in-vessel components of ITER is calculated for the basic-performance-phase for the reference PFM choice. Results are summarized in Fig. 23 where the bracket of uncertainty is indicated by the square. Thus for the baseline case, the total mobile inventory is found to be between 1050 g and 2200 g T while the trapped inventory is estimated in the range 530 g to 2400 g T. Because of safety concerns, the codeposited inventory (assumed mobilisable in the event of a breach in the double confinement barrier of the vessel and cryostat) should be limited to < 1 kg T, implying that an efficient clean-up method needs to be used whenever this value is reached.

Recent experiments on codeposition of C and Be with T carried out and documented by Mayer et al. [47] at low temperatures < 373 K and by Causey [48] in a range of temperature 373–573 K, show that T codeposits also with Be at a level similar to what is observed for C at 373 K. However, for Be the ratio of hydrogen isotopes drops to a few % already at temperatures of 500–600 K [49]. The level of impurity (mainly C and O) contained in the redeposited layers plays a strong role for co-depositing tritium with Be. The quantification of tritium codeposition on the divertor and adjacent surfaces is being studied in detail for ITER in connection with the overall erosion and lifetime analysis. Preliminary results of this analysis are discussed by Brooks et al. [49]. Computations have been performed for Be, CFC and W divertor plates showing similar amounts of T codeposition for CFC and Be (H/Be = H/C ~ 10%) below 300°C. In contrast to Be targets, tritium codeposition rates for CFC targets were found to be very high for detached conditions (~ 20 g T/1000 s discharge), due to build-up of chemically sputtered carbon on relatively cold surfaces in the divertor cassette. For semi-detached solutions (8 to 30 eV plasma in front of target) the codeposition rate is ~ 10 times lower and approximately equal for Be and CFC. Both erosion and tritium codeposition are essentially nil for tungsten in all the regimes studied.

Based on the results of these analyses and of experimental results confirming the buildup of codeposited layers it is clear that a reliable and efficient cleaning method is needed. Only glow-discharge cleaning, using He containing some oxygen has been so far used in existing machines. However, the rather low cleaning efficiency anticipated for ITER conditions and the resulting residual oxygen contamination of the plasma facing surfaces raises some concern. R&D is presently in progress in the EU home team to find alternative cleaning techniques based on e.g., controlled baking of the surfaces in air. Another promising approach is the addition of dopants to C-based materials (e.g., B, Si, Ti) which reduces the chemical erosion and therefore also can mitigate the codeposition problem. So far best results are obtained for Si-doped CFC

[50]. Even though encouraging, the reduced value of the sputtering yield is insufficient to eliminate the concern.

As far as tritium permeation is concerned, earliest breakthrough into the coolant (during year 6 and reaches 60 g T/yr) occurs for the lower portion of the baffle if protected by beryllium. For the baseline choice of PFM's in the divertor and for the baffle which are subject to high particle fluxes no permeation in the ITER lifetime was found.

4.5. Bakeout requirements for the in-vessel components

The temperature required for an efficient bakeout of plasma facing components protected with C-based materials is in the range of 300–350°C while lower temperatures ~ 200°C, are typically required for metals. The relatively high temperature in the case of CFC is needed to remove the adsorbed (mainly chemisorbed) water efficiently from the large inner surfaces of carbon-base armors (e.g., BET 0.1–1 m^2/g). They can absorb as much as 0.1 Pa m^3 of water per gram during exposure to air at room temperature. Experience in operating tokamaks with C-walls (i.e., JET, JT-60) shows that after air exposures and major in-vessel water leaks, high-current plasma operations could be resumed after 2 to 3-day bakeout periods at temperatures greater than 300°C. Much longer bake-out times are required when the walls are kept at lower temperature. In ITER, the baking temperature is limited to ~ 240°C (maximum temperature for water pressure of ~ 4 MPa). However, due to the fact that CFC is presently only considered for a relatively small area in the divertor (< 100 m^2) while the rest of the PFC's are clad with metals a bakeout temperature of 240°C seems acceptable, particularly considering ITER's long pulse length (≥ 1000) during which the temperature of the PFM's in the divertor will substantially exceed 300°C. Also during the transition from limiter to a divertor configuration it is expected that the higher impurity retention of the divertor compared with a limiter would mitigate the impurity influx expected from a weakly conditioned surface. If however, the limiter and the baffle

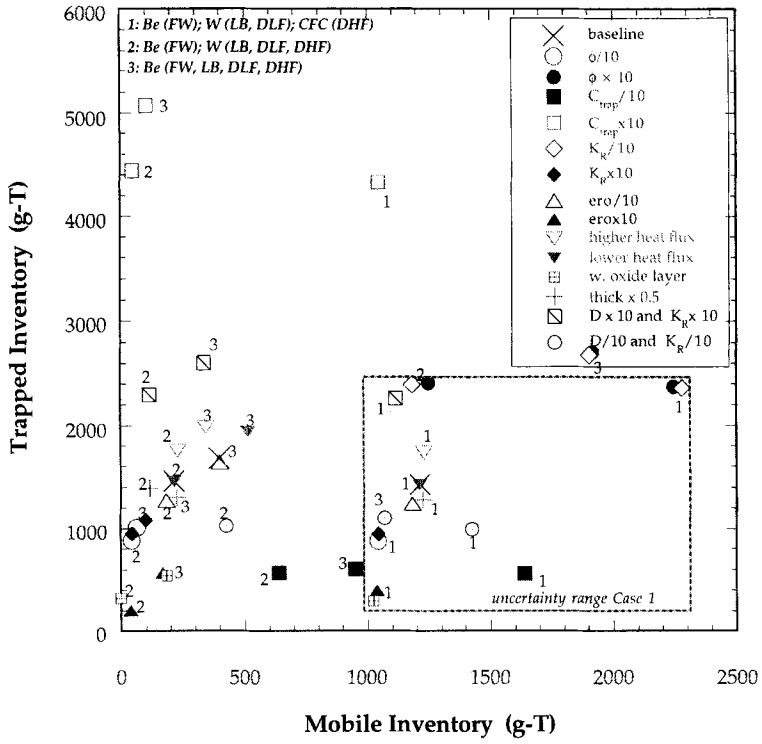

Fig. 23. Trapped inventory versus mobile inventory. Numbers in the figure refer to the various design options analyzed. (Abbreviations: FW = first wall, LB = lower baffle, DLF = low flux portion of divertor, DHF = high flux portion of divertor. The symbols in the legend are: ϕ-particle flux, C_{trap} = concentration of n-induced traps, K_R = surface recombination coefficient, ero = armor erosion rate, D = diffusion coefficient. Other cases analyzed refer to higher and lower (factor of 2) heat flux than the design value, thinner armor, and the presence of an oxide layer on the surfaces of the first wall, upper baffle, start-up limiter, and the low flux portion of the divertor that could strongly reduce the flux of tritium atoms migrating into the bulk and therefore mitigate the inventory. Further details can be found in Ref. [43].

would be clad with CFC, either higher bakeout temperatures or longer bakeout times may be required.

4.6. Dust in ITER, a safety issue

Plasma wall interactions in ITER with materials such as Be, W, and CFC's are expected to generate substantial amounts of 'dust'. This dust would be tritiated, radioactive, chemically reactive and/or toxic. In addition, there is the concern that its high surface area promotes reactions with steam during a water leak (Be-dust) producing sizeable quantities of hydrogen or gives rise to the possibility of explosions during sudden air leaks (carbon dust explosion). Therefore, methods are required to measure the quantity of dust inside the ITER machine and to remove it during maintenance periods. The impact of dust on machine safety depends on the material, on the size of the dust particles and on the total amount. For materials like Be and C the size of the dust particles determines the allowable quantity before removal has to take place ($\sim$ 10 kg to 100 kg for particle sizes of 10 μm to 100 μm, respectively).

A JCT-coordinated effort is ongoing to survey data available on dust production rates and characteristics of particle size and chemical composition in existing tokamaks, plasma simulation devices, high heat flux test beds and disruption simulation facilities. This work is taking account of all the experience available on Be in the joint European torus (JET), as well as other fusion devices where Be has been employed (such as ISX-B). Linear plasma simulators like PISCES and TPE as well as the JET neutral beam test bed will also add valuable insight. Experience from a tokamak with high-Z materials (Alcator C-Mod), high-Z probes included in DIII-D, and perhaps some preliminary experience available from plasma-sprayed tungsten coatings in ASDEX Upgrade will also be included. As far as graphite and CFC's are concerned, data on dust production and accumulation from TFTR, JET, DIII-D, and JT-60 will be evaluated as well as results from various disruption simulators and high heat flux test facilities in the Russian Federation.

However, to evaluate the amount of dust production in different devices does not allow by itself to extrapolate to ITER if the production mechanisms are not understood. Several mechanisms such as evaporation during disruptions, arcing, flaking of co-deposited layers, etc., are presently being discussed. The overall importance of each of these mechanisms as well as their relation to different operation conditions has to be investigated. In parallel dust diagnostics methods for ITER have to be developed which allow to determine the dust content in the machine with an accuracy of $\sim \pm 5$ kg having a lower detection limit of < 10 kg. Finally, methods of dust removal must be developed in order to periodically remove such dust whenever the level exceeds that at which the risk of a dust-related accident becomes unacceptably high.

5. Summary and conclusions

In this paper, a comprehensive overview of the designs of the main ITER in-vessel components, the divertor and first-wall/shield and related systems, has been presented. With two years remaining in the EDA, these designs continue to evolve, becoming more detailed and better supported by continued analysis and results from the R&D program. R&D has a longer lead time than design, and much of the R&D that was started shortly after the beginning of the EDA and which will ultimately provide the underlying technological basis for the ITER design is just now beginning to bear fruit. One can therefore expect a significant strengthening of the design basis on both the physics and technology sides during the remaining two years of the EDA.

Regarding the problem of heat and particle removal, thought by many at the beginning of the EDA as perhaps the most critical from the physics viewpoint, very substantial progress has been made and there is a growing confidence that the design approach described here represents a robust and effective solution. The progress made on this problem during the EDA is in no small measure due to the intensive R&D launched by the divertor physics community shortly after the EDA began. As 'second generation' experiments begin producing results during the next two years, it is anticipated that the ITER divertor design concept will be confirmed, in particular the ability of highly baffled divertors to maintain good confinement at $Z_{\text{eff}} \leq 1.6$ while radiating a substantial fraction of the heating power. The flexibility of the cassette approach, and the emphasis given in the design to efficient remote handling procedures, ensures that the new developments and insights that will undoubtedly come from the worldwide effort on divertor physics and related technology can be implemented into the ITER divertor concept at stages well into the basic performance phase.

The emphasis given in this paper to the effects of disruptions on the design of the divertor and first-wall/shield systems is fully indicative of their importance. Until recently, disruption mitigation and avoidance have not been given a particularly high priority for study within the tokamak physics community. Yet as discussed here, disruptions are the determining factor in the mechanical design of all in-vessel systems and with present understanding they tend to stress key components such as the shield module attachment, backplate, and divertor wings and cassette body to or even somewhat beyond nominal design limits. Further refinement to the modelling and to the design will reduce these stresses and bring them to acceptable levels even for 'worst case' disruptions. However it is clear that confidence in reaching the goals of the BPP and especially the EPP would be greatly enhanced if effective disruption avoidance and mitigation procedures were developed. A very promising start in this direction has been made by development of 'killer pellets' which

have experimentally been shown to be capable of reducing halo currents by at least a factor of 2. Proven and reliable mitigation measures such as this would be a most welcome development, not only by the designers of in-vessel systems, but also by the experimentalists and other users who will eventually operate and exploit ITER.

References

[1] ITER Interim Design Report (San Diego Joint Work Site, San Diego, 1995).

[2] S. Kaye et al., Plasma Physics and Controlled Nuclear Fusion Research, Proc. 15th Int. Conf., Seville (1994).

[3] G. Janeschitz, K. Borrass, G. Federici et al., J. Nucl. Mater. 220–222 (1995) 73–88.

[4] D.E. Post, J. Nucl. Mater. 220–222 (1995) 143–157.

[5] G.F. Matthews, J. Nucl. Mater. 220–222 (1995) 104–116.

[6] S. Allen, N. Brooks, R. Campbell et al., J. Nucl. Mater. 220–222 (1995) 336–341.

[7] O. Gruber, A. Kallenbach, M. Kaufmann et al., Phys. Rev. Lett. 74(21) (1995) 4217–4220.

[8] M. Nagami and the JT-60 Team, J. Nucl. Mater. 220–222 (1994) 1–12.

[9] B. Lipschultz, J. Goetz, B. LaBombard et al., J. Nucl. Mater. 220–222 (1995) 50–61.

[10] M.A. Mahdavi, S.L. Allen, D.R. Baker et al., J. Nucl. Mater. 220–222 (1995) 13–24.

[11] J. Neuhauser, M. Alexander, G. Becker et al., Plasma Phys. Controlled Fusion 37 (1995) A37–A51.

[12] M. Keilhacker, Plasma Phys. Controlled Fusion 37 (1995) A3–A17.

[13] J. Goetz, C. Jurz, B. LaBombard et al., Phys. Plasmas, Louisville, APS Meeting (1996).

[14] A. Allen, A. Bozek, N. Brooks et al., Plasma Phys. Controlled Fusion 37 (1995) A191–A202.

[15] B. Lipschultz, J. Goetz, I. Hutchinson et al., Proc. 22nd Eur. Phys. Soc. Conf. on Controlled Fusion and Plasma Physics 19C, Part III (1995) pp. 325–328.

[16] T. Petrie, D. Buchenauer, D. Hill et al., J. Nucl. Mater. 196–198 (1992) 849–853.

[17] R.J. Fonck, M.G. Bell, K. Bol et al., J. Nucl. Mater. 128–129 (1984) 330–339.

[18] D.E. Post, B. Braams, J. Mandrekas et al., Proc. 12th Int. Conf. on Plasma Surface Interactions in Contr. Fusion Devices, St. Raphael, J. Nucl. Mater. (1996), to be published.

[19] J. Mandrekas, W. Stacey and F. Kelly, Nucl. Fusion (1996), to be published.

[20] T. Rognlien, J. Milovich, M. Rensink et al., J. Nucl. Mater. 196–198 (1992) 347–351.

[21] B. Braams, Report No. EUR-FU IXII-80-87-68 (1987).

[22] P. Stangeby, J. Elder, D. Reiter et al., Contrib. Plasma Phys. 34 (1994) 306–311.

[23] A. Kukushkin, H.D. Pacher, M. Baelmans et al., Proc. 12th Int. Conf. on Plasma Surface Interactions in Contr. Fusion Devices, St. Raphael, J. Nucl. Mater. (1996), to be published.

[24] R. Schneider, D. Reiter, H.P. Zehrfeld et al., J. Nucl. Mater. 196–198 (1992) 810–815.

[25] A. Loarte, Proc. 12th Int. Conf. on Plasma Surface Interactions in Contr. Fusion Devices, St. Raphael, J. Nucl. Mater. (1996), to be published.

[26] D. Post, A. Kukushkin, R. Schneider et al., Plasma Physics and Controlled Nuclear Fusion Research, Proc. 15th Int. Conf. Seville (1994).

[27] M.E. Fenstermacher, G.D. Porter, M.E. Rensink et al., J. Nucl. Mater. (1994), to appear.

[28] G. Vlases, G. Corrigan and A. Taroni, Proc. 12th Int. Conf. on Plasma Surface Interactions in Contr. Fusion Devices, St. Raphael, J. Nucl. Mater. (1996), to be published.

[29] H. Nakamura, T. Hirayama, Y. Koide et al., Phys. Rev. Lett. 67(19) (1991) 2658–2659.

[30] C.C. Klepper, J.T. Hogan, P.K. Mioduszewski et al., J. Nucl. Mater. 196–198 (1992) 1090–1095.

[31] S.I. Krasheninnikov, A.S. Kukushkin and T.K. Soboleva, Nucl. Fusion 31(8) (1991) 1455–1470.

[32] G. Janeschitz, A. Antipenkov, S. Chiocchio et al., Plasma Physics and Controlled Nuclear Fusion Research, Proc. 15th Int. Conf. Seville (1994).

[33] J. Schlosser, private communication.

[34] J.A. Snipes, R.L. Boivin, C. Christensen et al., Phys. Plasmas 3(5) 1996.

[35] H. Nakamura, G. Federici, J. Andres et al., Status of ITER fuelling system design, to be presented at SOFT 96, Lisbon, September (1996).

[36] M.J. Gouge, W.A. Houlberg, S.E. Attenberger et al., Fusion Technol. 28(11) 1995.

[37] J.A. Goetz, C. Kurz, B. LaBombard et al., Phys. Plasmas 3(5) 1996.

[38] K. Ioki, L. Bruno, A. Cardella et al., Phys. Scr. (1996), to appear.

[39] A.R. Raffray and G. Federici, Raclette: A model for evaluating the thermal response of plasma facing components to slow high power plasma transients, Garching ITER Joint Work Site internal report (Garching, 1996).

[40] H.D. Pacher, I. Smid, G. Federici et al., Proc. 12th Int. Conf. on Plasma Surface Interactions in Contr. Fusion Devices, St. Raphael, J. Nucl. Mater. (1996), to be published.

[41] B.J.D. Tubbing et al., Proc. 22nd EPS Conf. Contr. Fusion and Plasma Physics, Bournemouth, III-453 (1995).

[42] H.D. Pacher and I. Smid, Net Internal Note N/1/3340/1/A, Garching (1996).

[43] G. Federici, D. Holland, G. Janeschitz and C.H. Wu, Proc. 12th Int. Conf. on Plasma Surface Interactions in Contr. Fusion Devices, St. Raphael, J. Nucl. Mater. (1996), to be published.

[44] G. Federici, D. Holland, J. Brooks et al., Preliminary Assessment of the Tritium Inventory and Permeation in the PFC's of ITER, SOFE 95.

[45] P.L. Andrew, A.T. Peacock and M.A. Pick, J. Nucl. Mater. 196–198 (1992) 997–1001.

[46] R.A. Causey, W. Harbin and R.A. Anderl, Proc. 12th Int. Conf. on Plasma Surface Interactions in Contr. Fusion Devices, St. Raphael, J. Nucl. Mater. (1996), to be published.

[47] M. Mayer, R. Behrisch, H. Plank et al., J. Nucl. Mater., to be published.

[48] R. Causey, personal communication.

[49] J.N. Brooks, R. Causey, G. Federici and D. N. Ruzic, Proc. 12th Int. Conf. on Plasma Surface Interactions in Contr. Fusion Devices, St. Raphael, J. Nucl. Mater. (1996), to be published.

[50] J. Roth, H. Plank and R. Schwörer, Proc. 7th Int. Work. on Carbon Mater., Stockholm, Sweden, September (1995).